Arctic Amplification Weakens the Variability of Daily Temperatures over Northern Middle-High Latitudes

AIGUO DAI^a AND JIECHUN DENG^{b,a}

^a Department of Atmospheric and Environmental Sciences, University at Albany, State University of New York, Albany, New York
^b Key Laboratory of Meteorological Disaster, Ministry of Education (KLME)/Joint International Research Laboratory of Climate and Environmental Change (ILCEC)/Collaborative Innovation Center on Forecast and Evaluation of Meteorological Disasters (CIC-FEMD), Nanjing University of Information Science and Technology, Nanjing, China

(Manuscript received 5 July 2020, in final form 14 October 2020)

ABSTRACT: Arctic amplification (AA) reduces meridional temperature gradients (dT/dy) over the northern mid-high latitudes, which may weaken westerly winds. It is suggested that this may lead to wavier and more extreme weather in the midlatitudes. However, temperature variability is shown to decrease over the northern mid-high latitudes under increasing greenhouse gases due to reduced dT/dy. Here, through analyses of coupled model simulations and ERA5 reanalysis, it is shown that consistent with previous studies, cold-season surface and lower-mid troposphere temperature (T) variability decreases over northern mid-high latitudes even in simulations with suppressed AA and sea ice loss under increasing CO₂; however, AA and sea ice loss further reduce the T variability greatly, leading to a narrower probability distribution and weaker cold or warm extreme events relative to future mean climate. Increased CO₂ strengthens meridional wind (v) with a wavenumber-4 pattern but weakens meridional thermal advection [-v(dT/dy)] over most northern mid-high latitudes, and AA weakens the climatological v and -v(dT/dy). The weakened thermal advection and its decreased variance are the primary causes of the T variability decrease, which is enlarged by a positive feedback between the variability of T and -v(dT/dy). AA not only reduces dT/dy, but also its variance, which further decreases T variability through -v(dT/dy). While the mean snow and ice cover decreases, its variability increases over many northern latitudes, and these changes do not weaken the T variability. Thus, AA's influence on midlatitude temperature variability comes mainly from its impact on thermal advection, rather than on winds as previously thought.

KEYWORDS: Advection; Climate models; Climate variability

1. Introduction

The Arctic region warms up about twice fast as the global mean in model simulations with increasing greenhouse gases (Holland and Bitz 2003; Collins et al. 2013; Barnes and Polvani 2015) and even more in recent observations (Serreze et al. 2009; Screen and Simmonds 2010; Cohen et al. 2014; Dai et al. 2019). This phenomenon, known as Arctic amplification (AA; Serreze and Barry 2011), occurs only in the cold season and mainly over areas with large sea ice loss (Screen and Simmonds 2010; Dai et al. 2019). AA reduces meridional temperature gradients (dT/dy, same as $\partial T/\partial y$ in this paper) in the lowermiddle troposphere, which leads to moderate weakening of the zonal wind (u) in the mid-upper troposphere (Dai and Song 2020). Because the strength of u is linked to atmospheric blocking (Luo et al. 2017, 2018; Yao et al. 2017) and other circulation fields, such as cyclonic activity (Murray and Simmonds 1995) and the jet-stream (Barnes and Screen 2015), it has been suggested that midlatitude circulation may become wavier because of AA, with more extreme weather caused by more frequent Arctic winter cold outbreaks (Francis and Vavrus 2012, 2015). However, the recently reported increase in midlatitude waviness (Francis and Vavrus 2015) has reversed its course and may not represent a response to GHG-induced global warming (Blackport and Screen 2020). Furthermore, recent observations and model simulations actually show

Corresponding author: Aiguo Dai, adai@albany.edu

reduced winter temperature (T) variability (for both daily and monthly T) over the northern mid-high latitudes under GHGinduced warming and sea ice loss due to smaller advectioninduced T anomalies associated with the weakened dT/dy(Stouffer and Wetherald 2007; Screen 2014; Ylhäisi and Räisänen 2014; Schneider et al. 2015; Holmes et al. 2016; Chen et al. 2019; Collow et al. 2019; Tamarin-Brodsky et al. 2020). This suggests that future midlatitude weather may become less variable and less extreme associated with sea ice loss during the cold season (Screen et al. 2015), in contrast to the waviness argument, which ignores the reduced advection-induced T anomalies. The waviness argument is based on an assumption that atmospheric jet stream and midlatitude u would weaken substantially while meridional wind (v) would strengthen under increasing GHGs, which are not supported by model results (Barnes and Polvani 2015; Barnes and Screen 2015; Dai and Song 2020). This implies that any recent increases in winter cold events (Westby et al. 2013; Cohen et al. 2014, 2020) may have resulted from internal variability (Koenigk et al. 2019), such as decadal changes in the occurrence frequency of the leading circulation patterns behind the T anomalies over Eurasia and North America (Deng et al. 2020) or anomalous atmospheric circulation patterns over North America (Luo et al. 2020), rather than a response to GHG-induced AA and sea ice loss (Dai and Song 2020).

Another source of uncertainty in many previous analyses of historical changes and fully coupled model simulations is the difficulty in separating the impact of AA and sea ice loss from the changes caused by either internal decadal variability or GHG-induced background warming. This is because many of these changes may be correlated and thus cannot be distinguished through regression or correlation analysis, as pointed out previously (Dai and Song 2020). Dai and Song (2020) recently used novel coupled model simulations to separate the AA's impact and found little influence from AA on midlatitude mean climate. The separation issue also exists in the previous studies on T variability change (e.g., Screen 2014; Ylhäisi and Räisänen 2014; Schneider et al. 2015; Chen et al. 2019; Collow et al. 2019; Tamarin-Brodsky et al. 2020), as these studies only examined the changes in observational and reanalysis data, or fully coupled model simulations that included the impacts from both the GHG-induced background warming and AA and sea ice loss. In other words, it is unknown from these studies how much of the T variability decrease is due to the AA and sea ice loss and how much is due to the GHG-induced background warming. Furthermore, the main mechanism for the T variability decrease identified in these previous studies is that the advection-induced T anomaly $[\approx -v(\partial T/\partial y)]$ will be smaller due to reduced dT/dyunder an implicit assumption that daily v and its variance would not change substantially. However, this assumption has not been verified, and this mechanism is used to explain the T variability decrease only in a qualitative sense. Partly because of these issues and deficiencies in model simulations (Screen et al. 2018; Dai and Song 2020), whether AA and Arctic sea ice loss would lead to more extreme weather over the northern midlatitudes is still debated (Francis 2017; Francis et al. 2017; Cohen et al. 2020).

In this study, we analyze October-March daily T, v, and other data from the ERA5 reanalysis and the novel coupled model simulations used in our recent studies (Dai et al. 2019; Dai and Song 2020) to address the following questions: 1) How does the surface and tropospheric T variability respond to increasing CO₂ even for cases with suppressed AA and Arctic sea ice loss? 2) In a fully coupled climate system, how much of the T variability decrease is due to AA and associated sea ice loss and how much is due to the background warming? 3) How does the daily v (including its variability) respond to increasing CO_2 and how does that affect T variability, as previous studies (Schneider et al. 2015; Holmes et al. 2016; Collow et al. 2019) have shown that the meridional advection term $-v(\partial T/\partial y)$ dominates T variability? And 4) Are there any additional processes besides the dT/dy-based mechanism that can help explain the T variability decrease in a quantitative sense under increasing CO₂? Answers to these questions should improve current understanding on how AA and Arctic sea ice loss may affect midlatitude weather and climate, and the T variability in particular.

Our results confirm previous findings (Screen 2014; Chen et al. 2019) that the variability of cold-season daily surface air temperature (Tas) over the northern mid-high latitudes decreases under increasing CO_2 . Our new findings suggest that the T variability decrease is initiated and peaks at the surface and propagates into the lower-mid troposphere, caused mainly by a reduction in the mean and variance of the meridional thermal advection -v(dT/dy). The T variability decreases

even in simulations with suppressed AA and Arctic sea ice loss, but the existence of large AA and sea ice loss would further reduce T variability greatly, rather than increasing it as argued previously based on AA's impact on v wind (Francis and Vavrus 2012, 2015). We also reveal a new zonal wavenumber-4 change pattern for v under increasing CO_2 that may enhance the background v; however, it is the change in -v(dT/dy), not v, that determines T variability response to CO_2 forcing. Because our focus is on AA's influence, which mainly affects dT/dy, and also because of the dominant role of -v(dT/dy) for temperature anomalies (Schneider et al. 2015), we only examined the role of meridional thermal advection in this study.

2. Data, model simulations, and analysis method

a. Data and model simulations

We analyzed the daily data for surface and atmospheric air temperature, v wind, sea ice concentration (SIC), snow cover, surface energy fluxes, and other fields from the European Centre for Medium-Range Weather Forecasts (ECMWF) reanalysis version 5 (ERA5) on a $2.5^{\circ} \times 2.5^{\circ}$ grid from January 1979 to March 2020 (Hersbach et al. 2020) and three coupled model simulations using the Community Earth System Model version 1.2.1 (CESM1) from NCAR (Hurrell et al. 2013). We ran the CESM1 with the CAM4 option, instead of CAM5, for its atmospheric component to reduce the computation associated with aerosols, which did not change in our simulations. The CESM1 was run with grid spacing of 2.5° longitude × $\sim 2.0^{\circ}$ latitude for the atmospheric model, and $\sim 1.0^{\circ}$ longitude $\times \sim 0.5^{\circ}$ latitude for the sea ice and ocean models. Previous studies (Jahn et al. 2012; Deser et al. 2015; Dai et al. 2019; Dai and Song 2020) have shown that the CESM1 simulates the Arctic and midlatitude mean climate fairly realistically, including the spatial and seasonal patterns of the sea ice and surface fluxes and their interannual variability. Like most coupled climate models, the CESM1-simulated daily T variability is comparable to reanalysis over most of the globe (Chen et al. 2019).

The three CESM1 simulations used here are described in detail and used by Dai et al. (2019) and Dai and Song (2020). They include a 150-yr preindustrial control run (CTL) with CO2 fixed at 284.7 ppmv, a 235-yr run with $1\% \text{ yr}^{-1} \text{ CO}_2$ increase (1%CO₂) starting from the preindustrial level with fully coupled dynamic sea ice, and another 235-yr run (FixedIce) that is the same as the 1%CO2 run except that all the internally calculated surface fluxes north of 30°N were applied to fixed sea ice cover interpolated from the CTL monthly climatology. The use of fixed sea ice cover for calculating surface fluxes in FixedIce run largely cuts off the two-way interactions between the atmosphere and sea ice, and it greatly suppresses Arctic sea ice loss and AA (Dai et al. 2019; Dai and Song 2020), making it an effective way to approximately fix SIC and eliminate AA under increasing CO₂ with minimal nonphysical intervention to the Arctic climate system. We emphasize that our prescribed sea ice fraction was used only in the coupler of the CESM1 for calculating (mainly for area-weighting) gridbox-mean fluxes; it



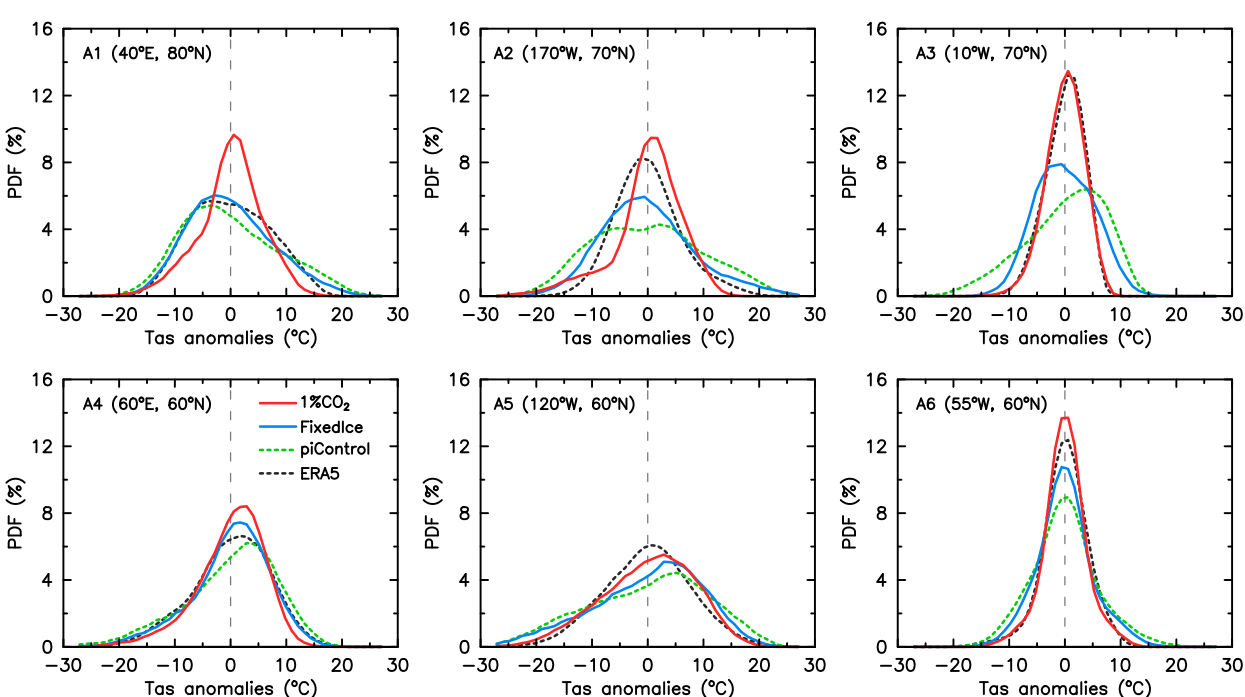


FIG. 1. Estimated PDFs of daily Tas anomalies during the cold season from October to March at six grid boxes in the northern mid-high latitudes. The x axis is the daily Tas anomaly (°C), and the y axis is the occurrence frequency (%). A fixed bin number of 52 was used for all the sites, and a five-point average was applied on all curves for clarity. Daily Tas anomalies are relative to the climatological mean for each calendar day for years 1979–2020 from ERA5 data (black dashed), years 31–80 from the control run (green dashed), and years 131–150 (around the second CO_2 doubling) from the $1\% CO_2$ (red solid) and FixedIce (blue solid) runs. The locations of the six selected grid boxes (A1–A6) are shown at the top-left corner of each panel and marked in Fig. 2a.

did not override or alter sea ice concentrations, sea ice fraction, or any other fields inside the ice model. Please see Fig. 9 in the supplementary information of Dai et al. (2019) for the sea ice cover in the CTL and FixedIce runs. More details about the FixedIce run, including its shortcomings, are provided in Dai et al. (2019) and Dai and Song (2020).

To study the impact of sea ice loss, many different approaches have been applied to maintain a near-constant Arctic sea ice cover in coupled model simulations, often with major nonphysical intervention to the Arctic climate system (such as adding an extra energy flux or changing sea ice albedo) (Screen et al. 2018; Dai and Song 2020; Sun et al. 2020). Our modeling approach focuses on the effects on the climate (including sea ice itself) of a fixed sea ice cover through its impact on surface fluxes, and by doing so it also largely eliminates the Arctic amplification of CO₂-induced warming (Dai and Song 2020). It provides a new way to maintain a near-constant sea ice cover with comparatively low nonphysical intervention.

Since AA and sea ice loss are largely suppressed in the FixedIce run (Dai et al. 2019; Dai and Song 2020), we can use this simulation to approximately represent the response to the background warming induced by the CO₂ increase without substantial AA and sea ice loss. In contrast, the standard 1% CO₂ run includes the responses to both the CO₂-induced background warming and AA together with sea ice loss, plus any nonlinear effects from them. Thus, the 1%CO₂-minus-

FixedIce difference approximately represents only the impact of AA and the associated sea ice loss (plus the nonlinear effects) under increasing CO₂. This allows us to roughly quantify the impact of AA and sea ice loss on mid-high-latitude weather and climate and compare it with that from the background warming alone (i.e., from FixedIce). In contrast, most previous studies on *T* variability examined simulations using a fully coupled system (like in our standard 1%CO₂ run) (Screen 2014; Schneider et al. 2015; Chen et al. 2019; Tamarin-Brodsky et al. 2020) or used atmospheric model simulations forced with specified SIC and sea surface temperatures (SSTs) (Collow et al. 2019); thus they are unable to separate the AA's impact from that resulting from local response and tropical influences on midlatitude *T* variability under increasing GHGs.

b. Analysis method

We focus on the cold season from October to March as AA is most pronounced during these months in both reanalysis data and model simulations (Dai et al. 2019; Dai and Song 2020). Daily averaged Tas, atmospheric temperature T, and other data from October 1979 to March 2020 from ERA5, years 31–80 from the CTL run, and a 20-yr period around the first ($2 \times \text{CO}_2$), second ($4 \times \text{CO}_2$), and third ($8 \times \text{CO}_2$) doubling of the preindustrial CO₂ from the $1\%\text{CO}_2$ and FixedIce runs were first converted into anomalies by removing the mean averaged over the respective time period for each day of the year. Please note

2594 JOURNAL OF CLIMATE VOLUME 34

that the CO₂-induced radiative forcing is proportional to the logarithm of its concentration, thus each doubling represents a twofold increase in its forcing. The resultant anomalies were used to estimate the probability density function (PDF) at select locations (Fig. 1) and to compute their standard deviation (SD) for each cold season at each grid box. Then, the SD was averaged over all the years to derive the mean SD for the given time period. We also computed the SD by combining the anomalies from all years together and the results are similar (not shown). As shown previously (e.g., Schneider et al. 2015; Chen et al. 2019) and by our own analysis (e.g., Fig. 1), the PDFs of the daily Tas anomalies are close to normal distributions, although some asymmetry is evident at certain locations (Fig. 1) and previous studies suggest an important role of the asymmetry for extremes (Garfinkel and Harnik 2017; Tamarin-Brodsky et al. 2020). Thus, SD still provides a good measure of Tas variability, although it may not be able to define the PDF completely (which is not our goal here) for some slightly skewed ones. Because we removed the mean seasonal cycle of the respective period, the mean warming is excluded in our analysis, as we focus only on the variability (relative to the respective mean climate). For daily v, dT/dy, v(dT/dy), and other variables, their local SD was similarly calculated, i.e., each variable [such as dT/dv or v(dT/dv)] was first converted into anomalies by removing its respective mean for each day and then the SD was calculated using the daily anomalies. Again, SD is used as a first-order measure of their variability, rather than to quantify their PDF changes.

Besides examining SD changes, we also analyzed the changes of the coldest (bottom five percentiles) and warmest (top five percentiles) Tas anomalies to further illustrate the PDF change. To quantify the contribution by the meridional thermal advection $[-v(\partial T/\partial y),$ referred to simply as -v(dT/dy) hereafter] to Tas variability, we also examined the SD change for this term and its individual components v and dT/dy. By decomposing the v and T into a mean and an anomaly component: $v = v_m + v_a$, and $T = T_m + T_a$ following Tamarin-Brodsky et al. (2019), the advection term can be decomposed into $-v(dT/dy) = -(v_m + v_a) \times d(T_m + T_a)/dy = -v_m \times (dT_m/dy) - v_m \times (dT_a/dy) - v_a \times (dT_a/dy)$. Thus,

$$\begin{split} \text{SD of} &- v(dT/dy) = \text{SD of} \left[-v_m \times (dT_m/dy) - v_m \times (dT_a/dy) \right. \\ &- v_a \times (dT_m/dy) - v_a \times (dT_a/dy) \right] \\ &= \text{SD of} &- v_m \times (dT_m/dy) + \\ &\quad \text{SD of} &- v_m \times (dT_a/dy) + \\ &\quad \text{SD of} &- v_a \times (dT_a/dy) + \\ &\quad \text{SD of} &- v_a \times (dT_a/dy) + \text{nonlinear terms.} \end{split}$$

The first term [SD of $-v_m \times (dT_m/dy)$] results from seasonal variations, the second (third) term is mainly due to daily variations in dT/dy (v), and the fourth term [SD of $-v_a \times (dT_a/dy)$] results from daily variations in both v and dT/dy. We computed these individual terms and examined their contributions to the total meridional thermal advection.

The variance of the dT/dy at a given grid box (i, j) with N temporal data samples may be calculated as

$$\begin{split} \mathrm{SD}_{dT/dy}^2 &= \frac{1}{N} \sum_{i=1}^N \left(\frac{\partial T_i}{\partial y} - \frac{\overline{\partial T}}{\partial y} \right)^2 \approx \frac{1}{N\Delta y^2} \sum_{i=1}^N \left(\Delta T_i - \Delta \overline{T} \right)^2 \\ &= \frac{1}{N\Delta y^2} \sum_{i=1}^N \left[\Delta (T_i - \overline{T}) \right]^2 \\ &= \frac{1}{N\Delta y^2} \sum_{i=1}^N \left[\frac{T_{i,j+1} - \overline{T}_{j+1} - (T_{i,j-1} - \overline{T}_{j-1})}{2} \right]^2 \\ &= \frac{1}{4N\Delta y^2} \sum_{i=1}^N \left[(T_{i,j+1} - \overline{T}_{j+1})^2 + (T_{i,j-1} - \overline{T}_{j-1})^2 \right. \\ &= \frac{1}{4N\Delta y^2} \sum_{i=1}^N \left[(T_{i,j+1} - \overline{T}_{j+1})^2 + (T_{i,j-1} - \overline{T}_{j-1})^2 \right. \\ &= \frac{1}{4\Delta y^2} \left[\frac{1}{N} \sum_{i=1}^N (T_{i,j+1} - \overline{T}_{j+1})^2 + \frac{1}{N} \sum_{i=1}^N (T_{i,j-1} - \overline{T}_{j-1})^2 \right. \\ &\left. - \frac{2}{N} \sum_{i=1}^N (T_{i,j+1} - \overline{T}_{j+1}) (T_{i,j-1} - \overline{T}_{j-1}) \right] \\ &= \frac{1}{4\Delta y^2} \left[\mathrm{SD}_{T_{j+1}}^2 + \mathrm{SD}_{T_{j-1}}^2 - 2 \left(\overline{T_{j+1}} T_{j-1} - \overline{T}_{j+1} \overline{T}_{j-1} \right) \right], \end{split}$$

where (i, j) are the longitude and latitude index, the overbar denotes the averaging over time and Δ is for finite differencing in the meridional direction. Thus, the variance of dT/dy is analytically related to the variance of T, and a decrease in the SD of T would lead to a decrease in the SD of dT/dy.

All changes in this study are relative to the control-run climatology. The $1\%\text{CO}_2$ -minus-FixedIce difference is computed and used to quantify AA's impact. A Student's t test with the 5% significance level was applied to test whether a change or difference in the mean of the SD at each grid box is statistically significant throughout the study.

3. Changes in T variability

Spatial characteristics

Figure 1 compares the PDFs of daily Tas anomalies at six select grid boxes (marked in Fig. 2a) in the northern mid-high latitudes (the focus of this study) from ERA5, the CTL run, and the $1\%\text{CO}_2$ and FixedIce runs around the time of the second CO_2 doubling. The CTL PDFs are similar to those from ERA5 at most of these locations, except at location A3 north of Iceland. The PDFs for the $1\%\text{CO}_2$ run are narrower with a sharp peak at all the locations (A1–A3 and A6) with large sea ice loss (Dai et al. 2019), while the narrowing is less pronounced over the two land locations (A4 and A5) in Eurasia and North America. Remarkably, the PDFs from the FixedIce run at $4\times\text{CO}_2$ differ only slightly from CTL, becoming slightly narrower.

The Tas SD changes (Fig. 2) confirm the above PDF changes, and show that the Tas variability decrease is widespread over the northern mid-high latitudes in both the 1%CO₂ and FixedIce runs, and is especially large over the areas with substantial sea ice loss (mainly in the 1%CO₂ run, Figs. 11a,b). Interestingly, even in the FixedIce run when sea ice loss and AA are small (at least around the first and second CO₂ doubling, Dai et al. 2019), Tas variability still decreases (by 2%–10% around the first CO₂ doubling) over most of the northern mid-high

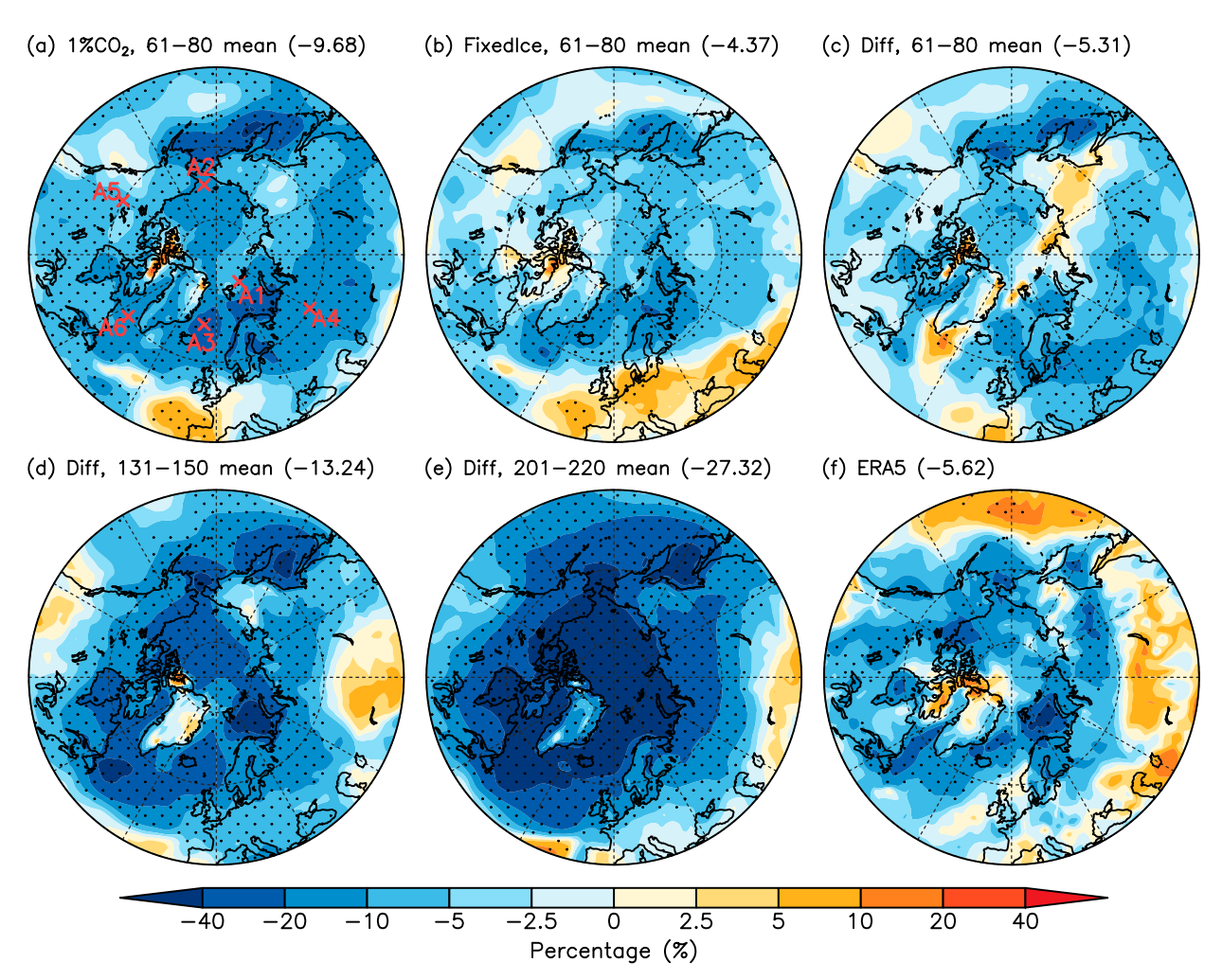


FIG. 2. CESM1-simulated October–March mean percentage change (% of and relative to the control climatology for years 31–80) in the standard deviation (SD) of daily Tas anomalies over $40^{\circ}-90^{\circ}$ N (same for all other maps). From the (a) $1\%\text{CO}_2$ and (b) FixedIce runs, and (c) their difference ($1\%\text{CO}_2$ minus FixedIce) around the time of the first CO₂ doubling (years 61–80). Red crosses in (a) mark the gridbox locations used in Fig. 1. (d) As in (c), but around the second CO₂ doubling (years 131–150). (e) As in (c), but around the third CO₂ doubling (years 201–220). (f) As in (c), but for the differences (% of the 1979–2020 climatology) between the 10 years with the lowest and highest Arctic sea ice cover (i.e., low minus high SIC years) based on ERA5 data during 1979–2020. The domain average is given on the top of each panel in parentheses. The stippling indicates the change or difference is statistically significant at the 5% level based on a Student's t test.

latitudes, including most of Eurasia and North America, but excluding central Europe when increases (Fig. 2b). However, the existence of large AA and sea ice loss in the $1\%\text{CO}_2$ run further reduces the Tas variability by an amount similar to that of FixedIce run (Figs. 2a–c), leading to large additional reduction ($\sim 10\%-40\%$ around the second CO₂ doubling and from $\sim 20\%$ to over 40% around the third doubling) in Tas variability, especially over the Arctic ocean (Figs. 2d,e). The composite difference between the low and high SIC years in ERA5 also shows widespread reduction of the Tas variability over most of the northern mid-high latitudes (Fig. 2f), qualitatively consistent with the model results. These results show that Arctic sea ice loss and the associated AA lead to greatly reduced Tas variability over the Arctic Ocean and other midto high-latitude areas, although the Tas variability also

weakens noticeably under increasing CO_2 even with suppressed sea ice loss and AA.

The reduction of daily *T* variability peaks at the surface and extends to the lower-mid troposphere, except for central Europe where the variability increases in the FixedIce run (Figs. 3 and 10e-h). Such a decreasing pattern with height in the changes for both *T* (Figs. 10a-d) and the SD of *T* suggests that these changes are caused by surface processes and then propagate upward, so that the signal weakens as it moves away from the source. Such a vertical pattern in AA has been noticed previously (e.g., Screen and Simmonds 2010; Dai et al. 2019) and used to argue that AA is caused mainly by changes in surface fluxes, namely, upward longwave (LW) radiation and sensible and latent heat fluxes from the newly opened warm Arctic waters during the cold season (Dai et al. 2019).

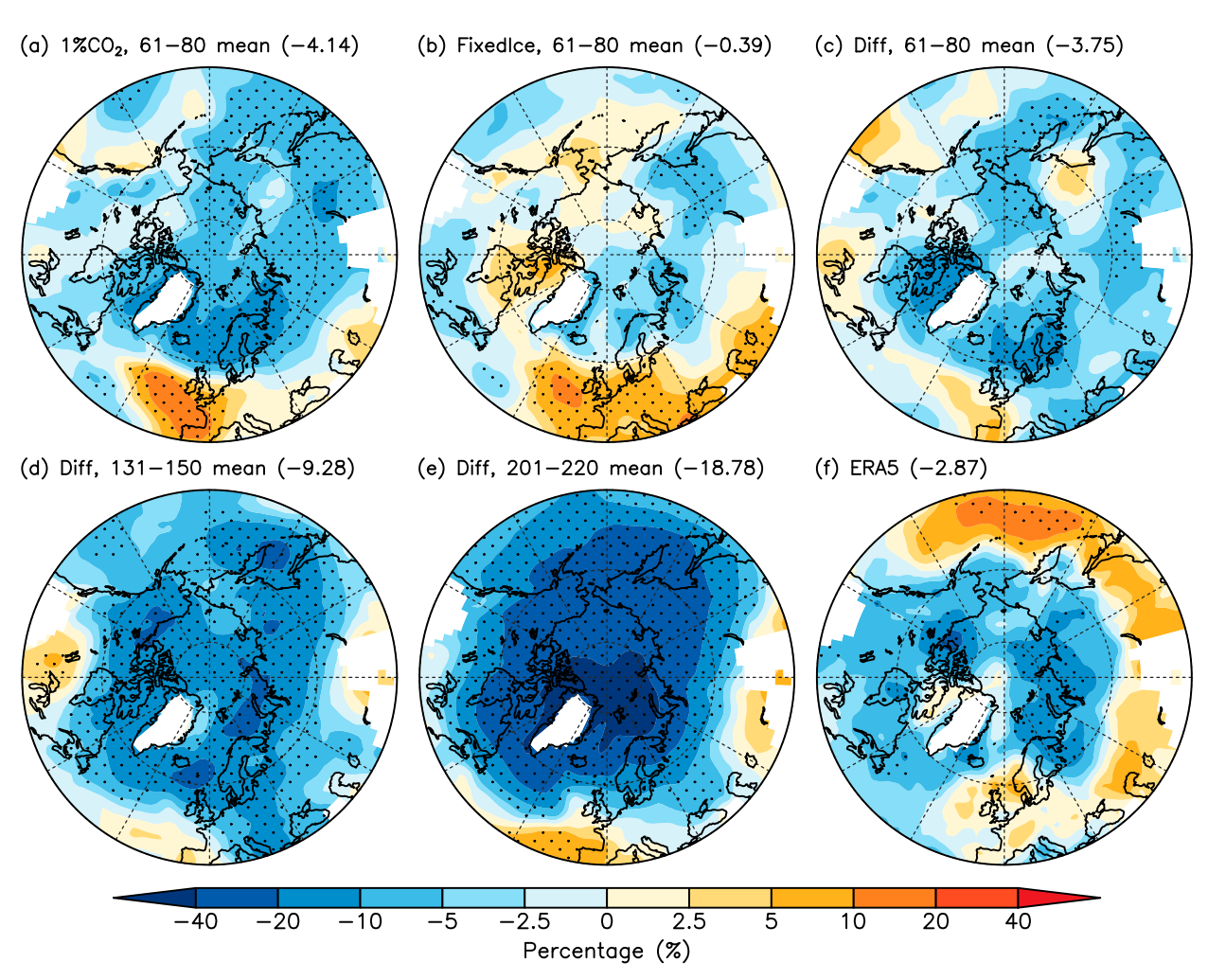


FIG. 3. As in Fig. 2, but for the SD of daily 850-hPa temperature anomalies, with elevated topography higher than 1400 m masked out as white.

As the PDFs of the daily Tas anomalies narrow and Tas variability decreases, the coldest and warmest days become less extreme than in CTL in both the standard 1%CO2 run with sea ice loss and AA and FixedIce run with suppressed sea ice loss and AA (Fig. 4). In other words, when the anomalies are defined relative to their respective mean climate (i.e., after removing the mean warming), future temperatures may in fact become less extreme under increasing CO₂ with or without the impact of sea ice loss and AA, contrary to the conventional view (Rahmstorf and Coumou 2011; Hansen et al. 2012) of increased extreme temperatures under GHG-induced global warming, as noticed previously (Huntingford et al. 2013). However, the mean warming would offset the impact of the reduced Tas variability and make any future hot days more extreme when compared with today's climate (Raghavendra et al. 2019), and the daily Tas variability does increase over the low latitudes (Chen et al. 2019).

Figure 4 also shows that AA and the associated sea ice loss would actually further weaken the Tas extremes, rather than increase them, especially over areas with large sea ice loss

(Figs. 11a,b) but also over many northern midlatitude regions. In other words, AA would make midlatitude temperatures less extreme as suggested previously (Screen et al. 2015), contrary to earlier arguments based on recent increases in midlatitude waviness (Francis and Vavrus 2012, 2015) that may not be part of the response to GHG increases (Blackport and Screen 2020).

4. Causes of the T variability decrease

Many studies have suggested that Arctic sea ice loss and the concurrent AA may have contributed to the Tas variability decrease over the northern mid-high latitudes (e.g., Huntingford et al. 2013; Screen 2014; Chen et al. 2019). In particular, Screen (2014) showed that because of the reduced dT/dy, local Tas anomalies associated with either northerly or southerly meridional wind v would decrease under increasing GHGs. For similar v, this would lead to reduced Tas variations. Chen et al. (2019) suggested that reduced sea ice cover would lead to less sea ice variability (in an absolute sense) and thus its



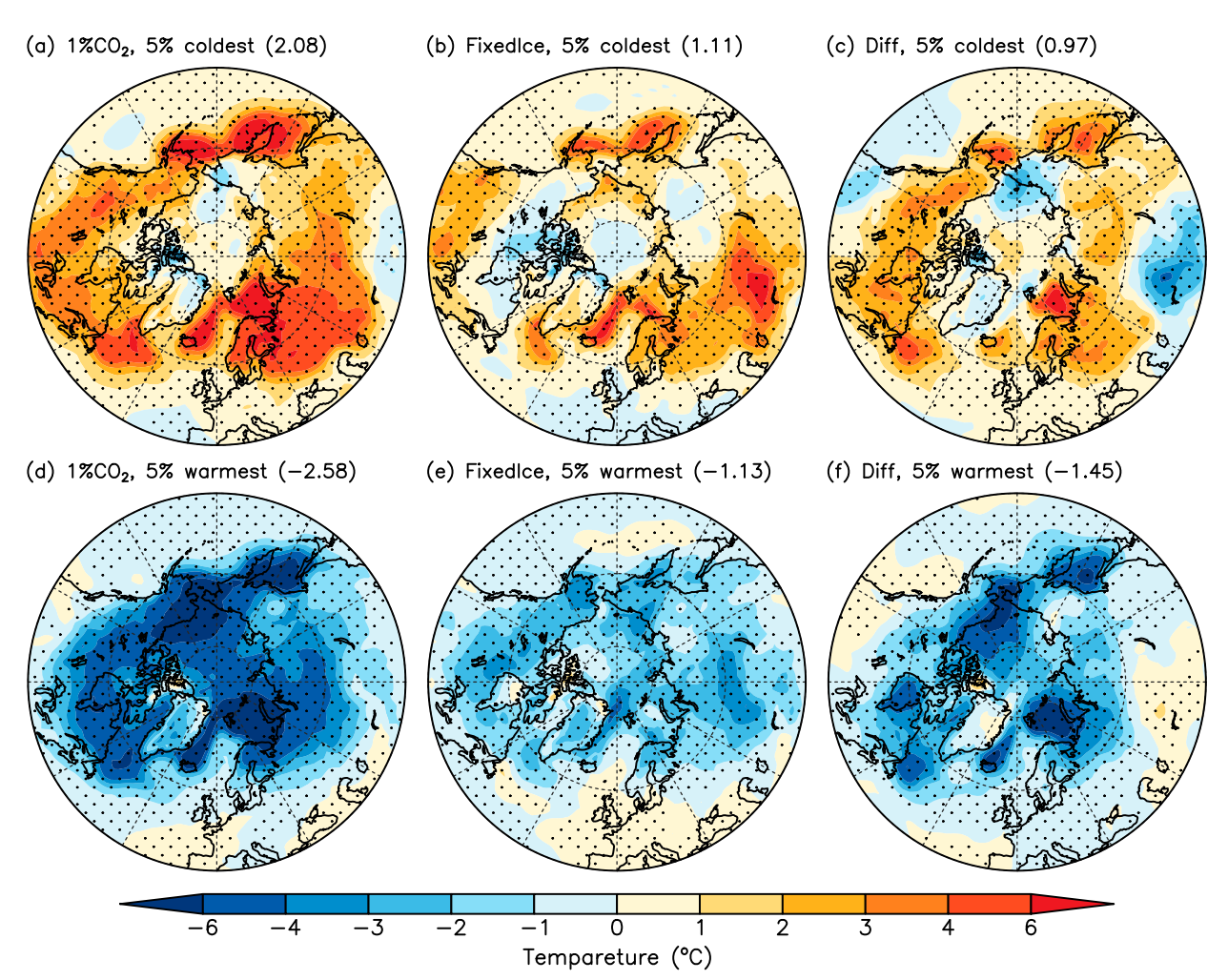


FIG. 4. CESM1-simulated changes (relative to the control climatology; $^{\circ}$ C) in the mean Tas anomalies (with the corresponding mean seasonal cycle removed) averaged over (top) the coldest (bottom five percentiles) and (bottom) warmest (top five percentiles) days for the (a),(d) 1%CO₂ and (b),(e) FixedIce runs and (c),(f) their difference (i.e., the 1%CO₂ minus FixedIce) around the time of the second CO₂ doubling (years 131–150). The domain average is given on the top of each panel in parentheses. The stippling indicates the change or difference is statistically significant at the 5% level based on a Student's t test.

ability to cause Tas variations, leading to reduced Tas variability directly over the Arctic Ocean and indirectly over nearby land through advection. However, how the combination of the υ and dT/dy changes and changes in other related fields, such as land snow cover and albedo, quantitatively contribute to the Tas variability decrease have not been examined so far. Furthermore, previous studies only analyzed the case where the impacts from both AA and the GHG-induced background warming (including local response and influences from low latitudes) are included. As a result, their individual impacts have yet to be quantified. In this section, we attempt to address these issues.

a. Impact of meridional thermal advection

Because of the large dT/dy compared with zonal temperature gradients dT/dx, the meridional thermal advection -v(dT/dy) plays a dominant role in determining local T

variations (Schneider et al. 2015; Deng et al. 2020). This is because $\partial T/\partial t = -v(\partial T/\partial y) - u(\partial T/\partial x) - w(\partial T/\partial z) + \text{local heating}$ term, and the meridional advection-induced daily anomaly $T' \equiv \Delta T = -v(\partial T/\partial y) \times \Delta t = -v(\partial T/\partial y)$ for $\Delta t = 1$ day (note $\partial T/\partial y$ is expressed simply as dT/dy in our text). Thus, changes in the mean of v and dT/dy are linked to T variations. For example, a weakened dT/dy would reduce local T anomalies associated with similar northerly or southerly winds (Screen 2014), leading to reduced T variability. Thus, we first examine their mean changes (color shading) in Fig. 5 at 850 hPa around the time of 4 × CO₂, together with their CTL climatology (contours). As expected, the positive dT/dy change in the 1% CO₂ run with decreasing sea ice would weaken the climatological dT/dy over most of the northern midlatitudes. In contrast, in the FixedIce run the dT/dy change (Fig. 5b) is negative over the northern North Atlantic, mid-high-latitude Eurasia and parts of the Arctic Ocean, which would enhance the

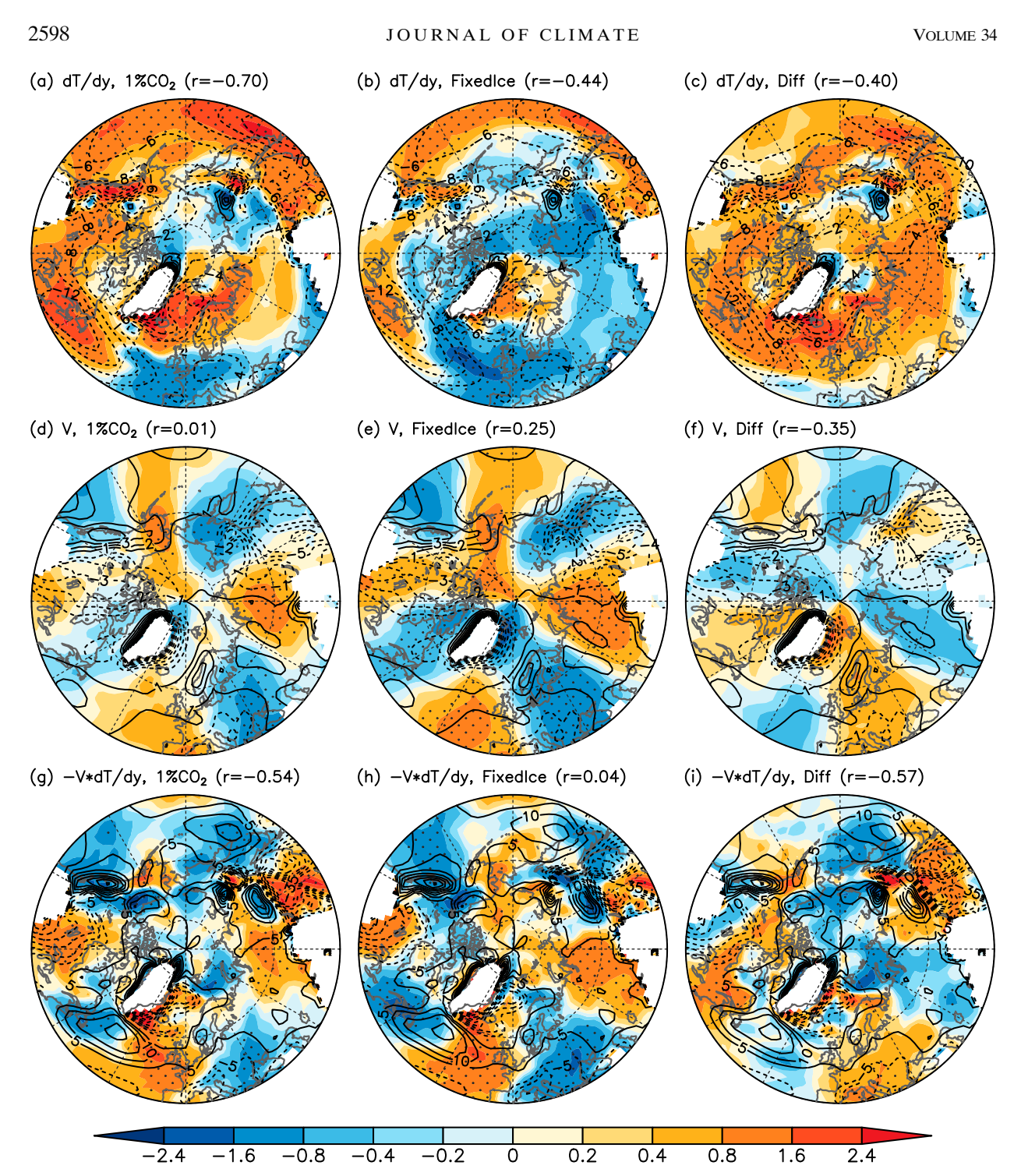


FIG. 5. CESM1-simulated October–March mean changes (relative to the control climatology) in the (top) meridional temperature gradient dT/dy (color shading; °C per 10° latitude), (middle) meridional wind v (color shading; m s⁻¹), and (bottom) meridional temperature advection $-v \times (dT/dy)$ (color shading; m s⁻¹ × °C per 10° latitude; scaled by a factor of 0.2 to use the same color table) at 850 hPa over 40°–90°N from the (a),(d),(g) 1% CO₂ and (b),(e),(h) FixedIce runs and (c),(f),(i) their difference (i.e., the 1% CO₂ minus FixedIce) around the time of the second CO₂ doubling (years 131–150). The contours are for the control climatology from years 31 to 80, at an interval of 2 in (a)–(c), 1 in (d)–(f), and 5 in (g)–(i); dashed contours are for negative values and the zero contour is omitted for clarity. The spatial pattern correlation coefficients between the contours and color shading within each panel are given at the top in parentheses. Areas with elevated topography higher than 1400 m are masked out as white. The stippling indicates the change or difference is statistically significant at the 5% level based on a Student's t test.

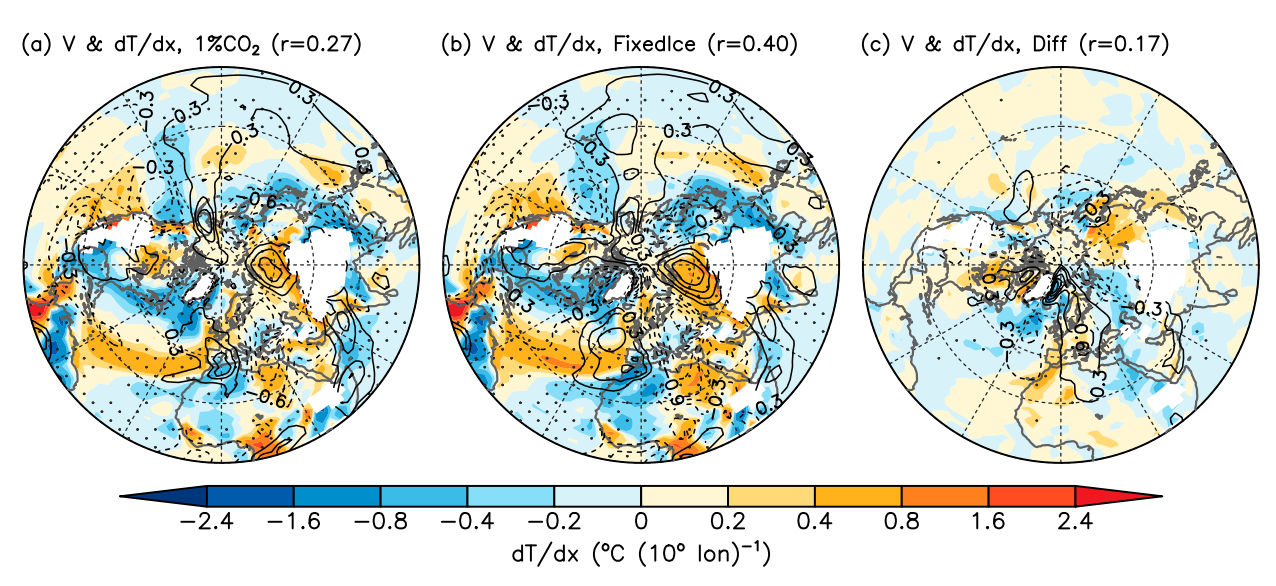


FIG. 6. CESM1-simulated October–March mean changes (relative to the control climatology) in 850-hPa zonal temperature gradient dT/dx (color shading; °C per 10° longitude) and meridional wind v (contours at an interval of 0.3 m s⁻¹; dashed contours are for negative values and the zero contour is omitted for clarity) over 0°–90°N from the (a) 1%CO2 and (b) FixedIce runs and (c) their difference (i.e., the 1%CO2 minus FixedIce) around the time of the second CO₂ doubling (years 131–150). The pattern correlation between dT/dx and v changes over 40°–90°N is given at the top of each panel in parentheses. Areas with elevated topography higher than 1400 m are masked out as white. The stippling indicates the colored change or difference is statistically significant at the 5% level based on a Student's t test.

background dT/dy. The enhanced dT/dy is a likely cause for the increased Tas variability over central Europe (Figs. 2b and 3b). As a result, the $1\%\text{CO}_2$ minus FixedIce difference (Fig. 5c) shows large positive dT/dy over most northern midhigh latitudes, confirming the notion that sea ice loss (through its impact on surface fluxes) leads to AA and reduced dT/dy (Dai et al. 2019).

The mean v changes (Figs. 5d–f) exhibit a zonal wavenumber-4 pattern with a very similar geographical phasing in both the $1\%\text{CO}_2$ and FixedIce runs, but with the latter having a stronger amplitude. This v change pattern extends from about 20° to 80°N (Fig. 6) and it is also seen at 500- and 250-hPa levels but not evident in the Southern Hemisphere (not shown). It seems to match the dT/dx change pattern well over the extratropical Northern Hemisphere (Fig. 6), and the dT/dx changes are mainly related to different warming rates over land and ocean. Thus, this wavenumber-4 response pattern for v likely partly results from the land–sea configuration in the Northern Hemisphere that leads to different warming rates and thus different dT/dx (Fig. 6), but this requires further investigations. The AA and sea ice loss in the $1\%\text{CO}_2$ run slightly weaken the dT/dx and v response to the CO_2 increase seen in the FixedIce run (Fig. 6).

Figures 5d-f also show that AA and sea ice loss (in the 1% CO₂ run) actually weaken the v response to CO₂ increases (in the FixedIce run), rather than making the flow wavier with stronger v as suggested previously (Francis and Vavrus 2012, 2015). The v wavenumber-4 response pattern shows negative v over Europe, East Asia, the eastern North Pacific, and eastern North America, but positive v over central Eurasia, the central North Pacific, central North America and the eastern North Atlantic, thereby enhancing the background v over central Eurasia, East Asia, the central North Pacific, eastern

North America and the eastern North Atlantic, but weakening it over Europe, the eastern North Pacific, and central North America (Figs. 5d,e). Thus, increased CO_2 enhances the meridional winds over most longitudinal sectors except Europe, the eastern North Pacific, and central North America; but the ν change resulting from AA and sea ice loss (Fig. 5f) weakens the background ν over most of the sectors except these three regions. Thus, overall, AA weakens meridional wind, contrary to previous notion that was based on recent increases in waviness (Francis and Vavrus 2012, 2015), while increased CO_2 generally leads to strong meridional winds over most longitudinal sectors.

The changes in meridional thermal advection -v(dT/dy)(Figs. 5g,h) are broadly similar in the two simulations and show a wave train pattern that roughly resembles the v change pattern, with small positive values over the central North Pacific. However, most of the changes have the opposite sign of the control climatology, leading to weakened meridional thermal advection. This differs from the v change that mostly enhances the control climatology. Because it is meridional thermal advection, not meridional wind, that affects local temperature anomalies and because their changes have nearly opposite signs, one should not use the enhanced regional v to infer that air temperatures will become more variable and extreme under increased GHGs, as is done in some previous studies. The AA and sea ice loss in the 1%CO₂ run weaken the response of -v(dT/dy) seen in the FixedIce run over most northern mid-high latitudes, especially over the continents (Figs. 5g,h), leading to weakening of the control climatology over most regions (Fig. 5i). Thus, despite the nonuniform difference patterns shown in Fig. 5i (in contrast to the uniformly positive dT/dy difference shown in Fig. 5c), AA and sea ice loss

still weaken the meridional thermal advection over most midhigh latitudes, which should lead to reduced temperature variations.

While the mean changes in dT/dy, v and -v(dT/dy) are relevant to T variations, it is the variance of daily -v(dT/dy) that is directly linked to local T variability. Figure 7g shows that the SD of daily -v(dT/dy) decreases by 5%–40% over most northern mid-high latitudes in the 1% CO₂ run around the time of $4\times$ CO₂, while it shows both increases and decreases in the FixedIce run (Fig. 7h). This results in ubiquitous decreases of 5%–40% over the northern mid-high latitudes due to AA and sea ice loss (Fig. 7i). The SD change and difference patterns for -v(dT/dy) match those of the SD of Tas (Figs. 2 and 3). Thus, the reduced variance in the meridional thermal advection plays a key role in the reduction of T variance.

Figure 7 further shows that most of the reduction in the variance of -v(dT/dy) results from reduced variance in dT/dy, with a small contribution from reduced variance in v (mainly over the North Atlantic, Europe and the eastern North Pacific). Increased CO_2 enhances the v variability slightly (by 2.5%-10%) only over East Asia and the Arctic Ocean (Fig. 7e), and AA weakens this response (rather than making v more variable), leading to reduced v variability over most northern latitudes (Fig. 7d). Thus, our model results suggest that AA would weaken both the mean and variance of meridional wind over most longitudinal sectors in northern mid-high latitudes, and this would not lead to increased variability in temperature. Instead, reduced variance in dT/dy, coupled with reduced variance in v over many parts of the northern latitudes, would lead to reduced variability in -v(dT/dy)and T. These model results are qualitatively consistent with the composite differences between low- and high-sea ice years in ERA5 (Fig. 8), which also shows reduced variance of -v(dT/dy)at many regions in the northern mid-high latitudes that comes mainly from the reduced variance in dT/dy as Arctic sea ice decreases.

Statistically, the SDs of dT/dy and of T are related to each other [see Eq. (2)]. Physically, as the local T becomes less variable, its meridional gradient should also become less variable since dT/dy approximately equals ΔT (a T difference in the meridional direction) divided by a constant Δy . Thus, the variance of dT/dy and T are linked. The reduced variance in dT/dy can further decrease the variance of -v(dT/dy) (Fig. 7) and thus the variance of T because the meridional advection-induced local T anomaly $T' = -v(\partial T/\partial y)$. This provides a positive feedback between the variance of T and the thermal advection: as the variance of T decreases (e.g., caused by reduced mean dT/dy under similar v), the variance of dT/dy would decrease, which would decrease the variance of T.

We also notice that even in the FixedIce run, where the negative climatological dT/dy strengthens over most of the high-latitudes and midlatitude Eurasia and the North Atlantic (Fig. 5b), the SD of dT/dy still decreases over many of these regions (Fig. 7b). This suggests that other factors (such as variance changes in T and v) besides the weakened mean dT/dy can also reduce the variance of dT/dy. On the other hand, the large enhancement of the negative mean dT/dy over central to

southern Europe (due to elevated warming over southern Europe, Figs. 5a,b) leads to increased SD of dT/dy over that region in both the 1%CO2 and FixedIce runs (Figs. 7a,b).

Using Eq. (1) in section 2, we can further decompose the SD of -v(dT/y) into contributions from the mean advection term $-v_m(dT_m/dy)$, the mean wind with anomaly T term $-v_m(dT_a/dy)$, the anomaly wind with mean gradient term $-v_a(dT_m/dy)$, and the anomaly wind with anomaly gradient term $-v_a(dT_a/dy)$ (Fig. 9). Here, the variations in the mean represent day-to-day variation in the mean annual cycle, while the anomaly variations include all the variations besides the mean seasonal variations; thus, we would expect the anomaly variations to contribute more to the SD of -v(dT/dy) than the mean. The top two rows of Fig. 9 show that most of the decrease in the SD of -v(dT/y) comes from the anomaly variations $-v_a(dT_a/dy)$, with some contribution from the anomaly wind with mean gradient term $-v_a(dT_m/dy)$, while the mean wind with anomaly gradient term $-v_m(dT_a/dy)$ would increase the SD. However, AA and sea ice loss reduce the thermal advection through all these terms (Fig. 9, bottom row).

The above changes in T, dT/dy, and the SD of T, dT/dy, v, and v(dT/dy) extend to the middle troposphere, with the largest changes near the surface (Fig. 10). Large AA and dT/dychanges are seen in the 1%CO2 run but they are small in the FixedIce run (Figs. 10a,b). The zonally averaged SDs of local daily T and dT/dy show similar decreasing patterns below about 500 hPa in both simulations, with a larger magnitude in the 1%CO2 (Figs. 10e,f). Thus, AA and sea ice loss further weaken the variability in lower-mid tropospheric T and dT/dyinduced by increasing CO₂ (Figs. 10e-g). Figures 10e-g also confirm that the SDs of T and dT/dy are closely linked, as explained above. Similarly, the SDs of v and -v(dT/dy) decrease in the lower-mid troposphere, with the decrease in the SD of v extending to the upper troposphere at lower latitudes (Figs. 10i,j). Again, AA and sea ice loss enhance these decreases in the 1%CO2 run, leading to large negative differences between the two runs (Fig. 10k). Interestingly, the SDs in the upper troposphere show some increase for T, dT/dy, v, and -v(dT/dy) (Fig. 10), suggesting different processes there. The ERA5 composite differences between the low and high sea ice years show reduced SDs for T, dT/dy, and -v(dT/dy)mainly north of \sim 50°N but little SD change for v (Figs. 10d,h,l). Given the large sampling uncertainties in the ERA5 composites, these patterns are broadly consistent with the CESM1simulated differences between the 1%CO₂ and FixedIce runs.

In summary, increased CO_2 generally strengthens meridional wind v but weakens meridional thermal advection -v(dT/dy) over most of the northern mid-high latitudes, and the existence of AA and sea ice loss (as in our $1\%CO_2$ run) weakens the climatological v and -v(dT/dy). The weakened thermal advection decreases T variability. The reduced T variability leads to lower variability for dT/dy, which in turn reduces the variability of -v(dT/dy), and the latter further reduces the T variability, generating a positive feedback loop between the variability decreases in T and the thermal advection. The AA's impact on midlatitude temperature variability comes mainly from its impact on thermal advection [through $-v_a(dT_a/dy)$ and $-v_a(dT_m/dy)$, Fig. 9], rather than its dynamic impact on

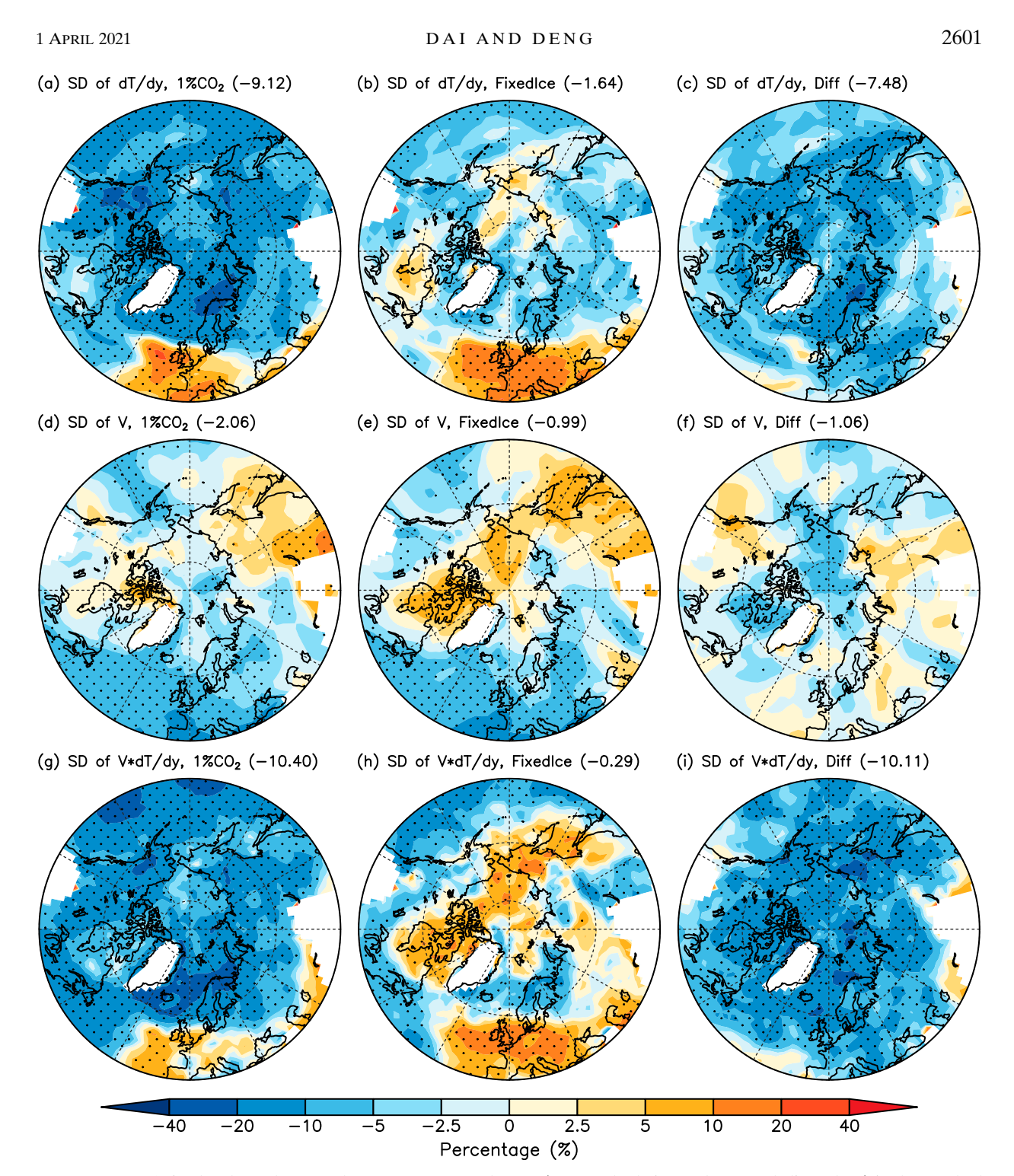
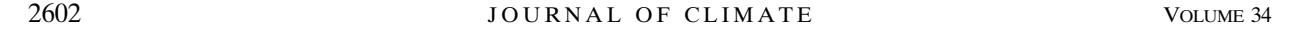


FIG. 7. CESM1-simulated October–March mean percentage changes (% of and relative to the control climatology) in the standard deviation (SD) of daily anomalies (with the corresponding mean seasonal cycle removed) in the (a)–(c) meridional temperature gradient dT/dy, (d)–(f) meridional wind v, and (g)–(i) meridional temperature advection $v \times (dT/dy)$ at 850 hPa over 40°–90°N from the (left) 1% CO₂ and (center) FixedIce runs, and (right) their difference (i.e., the 1%CO₂ minus FixedIce) around the time of the second CO₂ doubling (years 131–150). Areas with elevated topography higher than 1400 m are masked out as white. The domain average is given at the top of each panel in parentheses. The stippling indicates the change or difference is statistically significant at the 5% level based on a Student's t test.



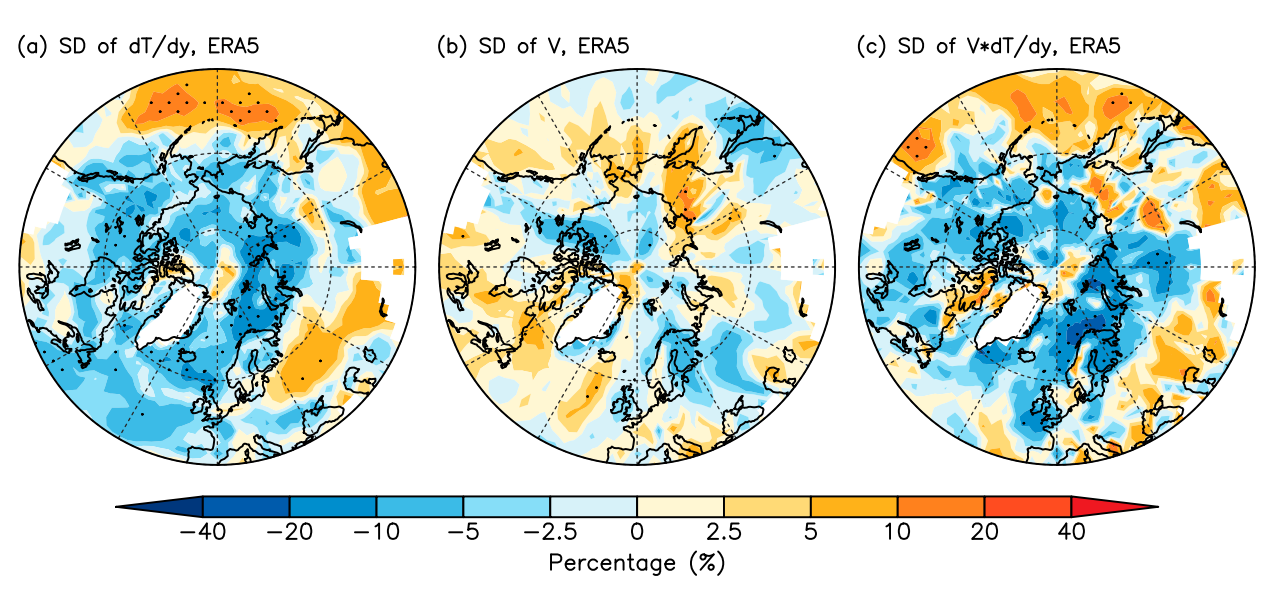


FIG. 8. As in Fig. 7, but for the differences (% of the 1979–2020 climatology) between the 10 years with the lowest and highest Arctic sea ice cover (i.e., low minus high SIC years) based on ERA5 data during 1979–2020.

winds, which was the focus of some previous studies (e.g., Francis and Vavrus 2012, 2015).

b. The impact of snow and ice cover changes

Besides the Arctic sea ice loss-induced amplification of the GHG-induced warming, changes in land snow and ice cover may also affect Tas variability. For example, air temperature over a snowpack may be more stable than over an ice-free surface due to the large heat capacity of the snowpack. Variations in snow and ice cover also alter surface albedo and thus net solar radiation, as well as surface turbulent heat fluxes, thereby affecting Tas variability. Figure 11 shows that mean snow and ice cover decreases everywhere in the mid-high latitudes (which continues to the third doubling of atmospheric CO₂; not shown), especially in the 1%CO₂ run when the impacts of sea ice loss on surface fluxes are included (Fig. 11a). Note that land snow cover and sea ice at lower latitudes (including the Hudson Bay) also decreases substantially in the FixedIce run (Fig. 11b), as the CO₂-induced warming are sufficient to melt them at those latitudes, in contrast to Arctic sea ice, where the CO₂-induced warming without large AA is insufficient to melt the ice in the FixedIce run. As a result, the largest difference in the SIC or snow cover (SC) between the two runs are seen in the Arctic (Fig. 11c), and the differences bear some similarity to the low-minus-high SIC composites in ERA5, particularly for subArctic and Arctic land areas (Fig. 11d).

As the mean SIC and SC decrease at lower latitudes, their variability also decreases; however, their variability at the high latitudes increases despite their mean decreases (Figs. 12a–c). This is likely due to the fact that melting at the lower latitudes greatly diminishes the snow cover to a very low value, leading to reduced variability there; but the melting at the high latitudes reduces the ice/snow cover to below 100%, making it more variable in time. The low-minus-high SIC composite

difference (Fig. 12d) in ERA5 bears some similarity to the CESM1-simulated difference (Fig. 12c), given the less warming and melting over the Arctic in current climate.

In theory, a reduced mean ice and snow cover coupled with their increased variability at high latitudes may reduce the insulation effect of the snow/ice layer and increase the surface albedo variations and thus variations in surface absorbed shortwave (SW) radiation, thereby leading to more Tas variability. Indeed, Figs. 13a and 13d show that the variability in surface net SW radiation increases over most of the mid-high latitudes under increasing CO₂ (with small changes in the Arctic in the FixedIce run). Thus, snow and ice cover changes (including their variability changes) cannot explain the decreases in Tas variability. For surface net LW radiation, its variability increases over areas with large sea ice loss (Fig. 13b, likely due to decreased insulation of the ice layer) but decreases over the North Pacific and Europe (Figs. 13b and 13e, likely related to decreased T variability there). The variability of surface turbulent heat fluxes increases in the Arctic in the 1%CO2 run (Fig. 13c) but decreases in the northern North Atlantic (Figs. 13c,f), with small changes over land. Thus, these LW and heat flux change patterns also do not match well with the widespread decreases in Tas variability, suggesting that they do not play a major role in causing the reduction in Tas variability.

The ERA5 composite differences between the years with low SIC and high SIC show generally increased variability for net SW radiation over most of the northern mid-high latitudes (Fig. 13j) and for the turbulent heat fluxes over the Arctic areas with large sea ice loss (Fig. 13l). These differences are qualitatively consistent with the model-simulated differences between the $1\%\text{CO}_2$ and FixedIce runs (Figs. 13g,i). The LW variability differences are mostly insignificant in ERA5 (Fig. 13k).

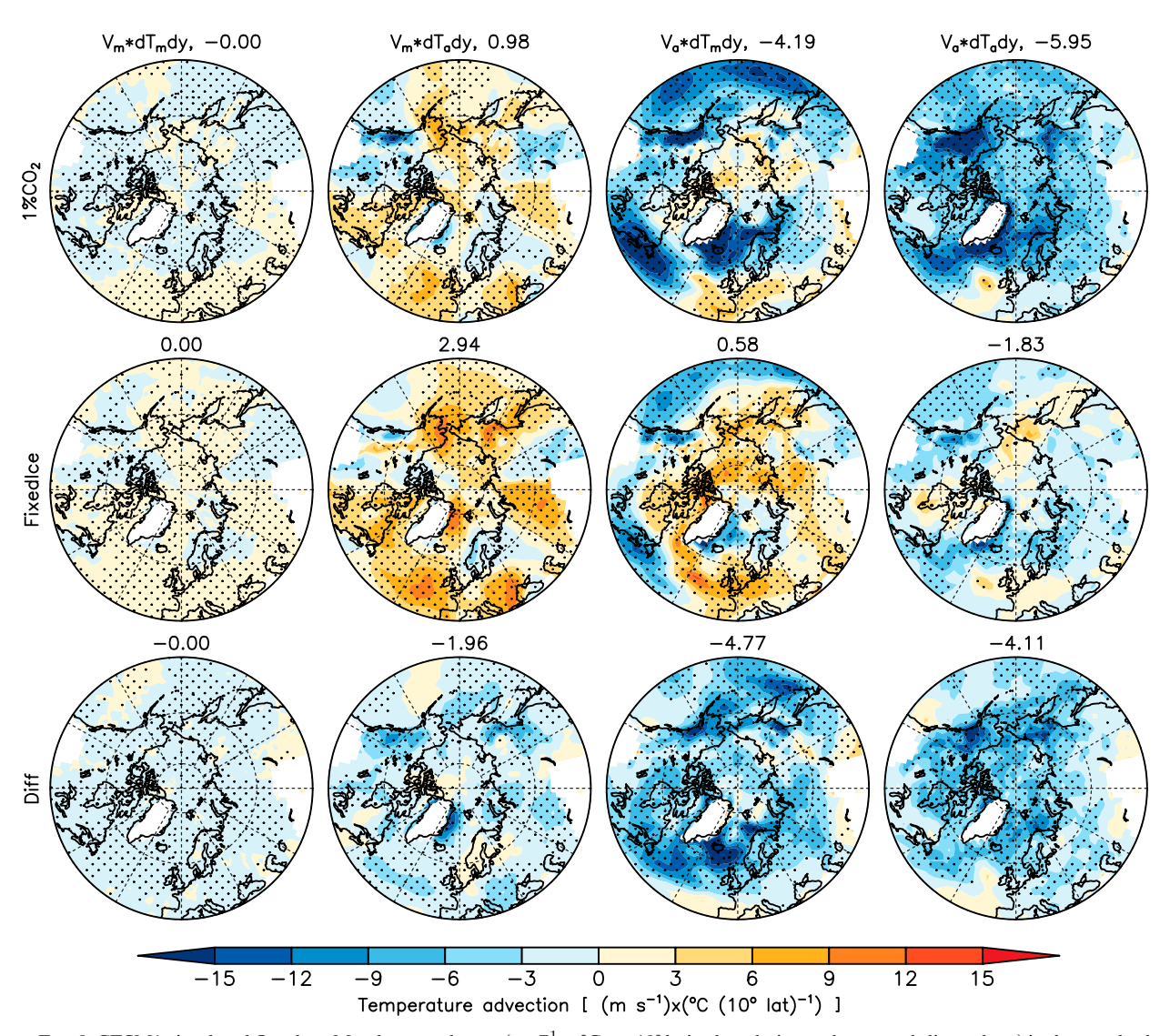


FIG. 9. CESM1-simulated October–March mean change (m s $^{-1}$ × $^{\circ}$ C per 10° latitude, relative to the control climatology) in the standard deviation (SD) of the daily anomalies (with the corresponding mean seasonal cycle removed) of four components (columns 1–4 from the left) of 850-hPa meridional temperature advection $v \times (dT/dy)$ from the (top) 1% CO₂ and (middle) FixedIce runs, and (bottom) their difference (1% CO₂ minus FixedIce) averaged over years 131–150 (around the second CO₂ doubling). Areas with elevated topography higher than 1400 m are masked out as white. The stippling indicates the change is statistically significant at the 5% level based on a Student's t test. The four components of the meridional temperature advection include $v_m \times (dT_m/dy)$, $v_m \times (dT_a/dy)$, $v_a \times (dT_m/dy)$, and $v_a \times (dT_a/dy)$, where the subscripts m and a indicate, respectively, the climatological mean and the daily deviation from this mean for each calendar day. To quantify the relative contribution of each term, all the changes are presented in their physical unit here. The domain average is given at the top of each panel.

5. Summary and conclusions

In this study, we have analyzed CESM1 model simulations and ERA5 reanalysis data to examine the impact of increasing CO_2 and the influence of the associated Arctic amplification (AA) and Arctic sea ice loss on the variability of daily air temperature T over the northern mid-high latitudes ($40^{\circ}-90^{\circ}N$) during the cold season from October to March. It is found that increasing CO_2 leads to reduced T variability at the surface and in the lower-mid troposphere, with the largest reduction near the surface. This occurs even in CESM1 simulations with

suppressed AA and Arctic sea ice loss, although the existence of AA and sea ice loss further decreases the T variability greatly, by a factor of \sim 2. The reduced T variability leads to a much narrower probability distribution and weaker cold or warm extreme events when they are defined relative to future mean climate. Consistent with several previous studies (Huntingford et al. 2013; Screen 2014; Schneider et al. 2015; Chen et al. 2019), these results suggest that northern midhigh-latitude cold-season temperatures may become less variable and less extreme in GHG-induced warmer climates,

2604 JOURNAL OF CLIMATE VOLUME 34

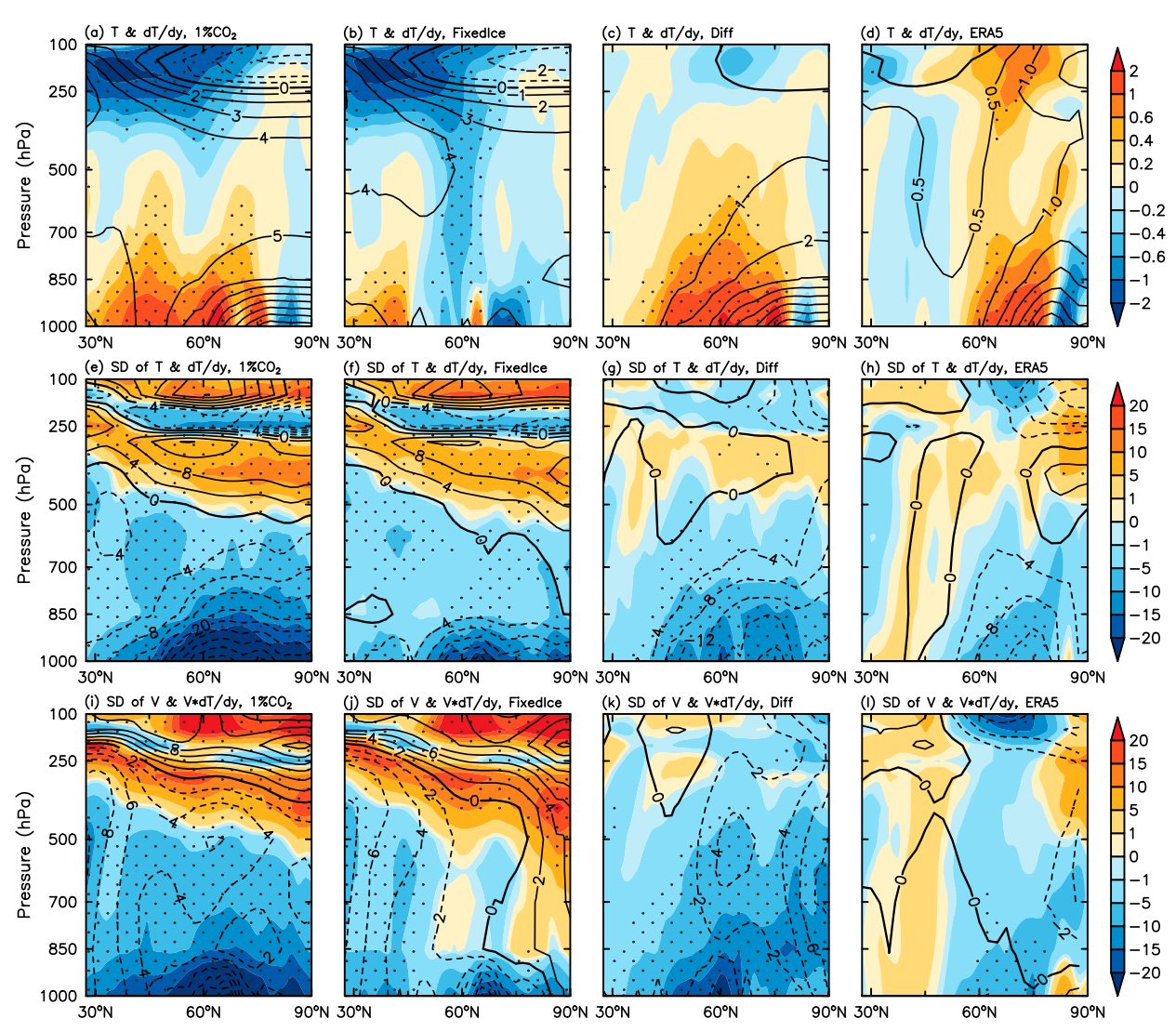


FIG. 10. CESM1-simulated October–March mean change (relative to the control climatology) in zonal-mean air temperature (contours; °C) and its meridional gradient (color shading; °C per 10° latitude) from the (a) 1%CO2 and (b) FixedIce runs, and (c) their difference (1%CO2 minus FixedIce) averaged over years 131-150 (around the second CO_2 doubling). (d) As in (c), but for the difference between the 10 years with lowest and highest Arctic SIC based on ERA5 data during 1979-2020. (e)–(h) As in (a)–(d), respectively, but for the percentage change or difference (% of the control-run climatology or ERA5 1979-2020 mean) in zonal-mean SD of daily anomalies (with their corresponding mean seasonal cycle removed) of air temperature (contours) and meridional temperature gradient (color shading). (i)–(l) As in (e)–(h), respectively, but for the percentage change or difference in zonal-mean SD of daily anomalies in meridional wind (contours) and meridional temperature advection (color shading). The contours are at an interval of 1°C in (a)–(c), 0.5°C in (d), 4% in (e)–(h), and 2% in (i)–(l); the dashed contours are for negative values. The stippling indicates that the colored change or difference is statistically significant at the 5% level based on a Student's t test. The mean temperature changes [contours in (a)–(d)] over about 0.5°C or below -0.5°C are statistically significant, while the mean SD changes of temperature [contours in (e)–(h)] and meridional wind [contours in (i)–(l)] over about 2% or below -2% are statistically significant.

contrary to the notion that temperature variability and extremes may increase in such a warmer climate (Rahmstorf and Coumou 2011; Hansen et al. 2012) and that AA may enhance midlatitude *T* variability by making the airflow wavier (Francis and Vavrus 2012, 2015).

We found that although increased CO_2 enhances meridional wind v over many northern mid-high-latitude regions (i.e., the airflow may indeed become wavier), it does not lead to increased T variability because the meridional thermal advection -v(dT/dy), which is more directly linked to T variations than v (as the advection-induced T anomaly $T' = -v(\partial T/\partial y)$), and its variance decrease under increasing CO_2 . Furthermore, the existence of large AA and Arctic sea ice loss, as seen in our $1\%CO_2$ run, weakens v and -v(dT/dy) and their variance and thus further decreases the T variability. The response of meridional wind to increasing CO_2 clearly shows a zonal wavenumber-4

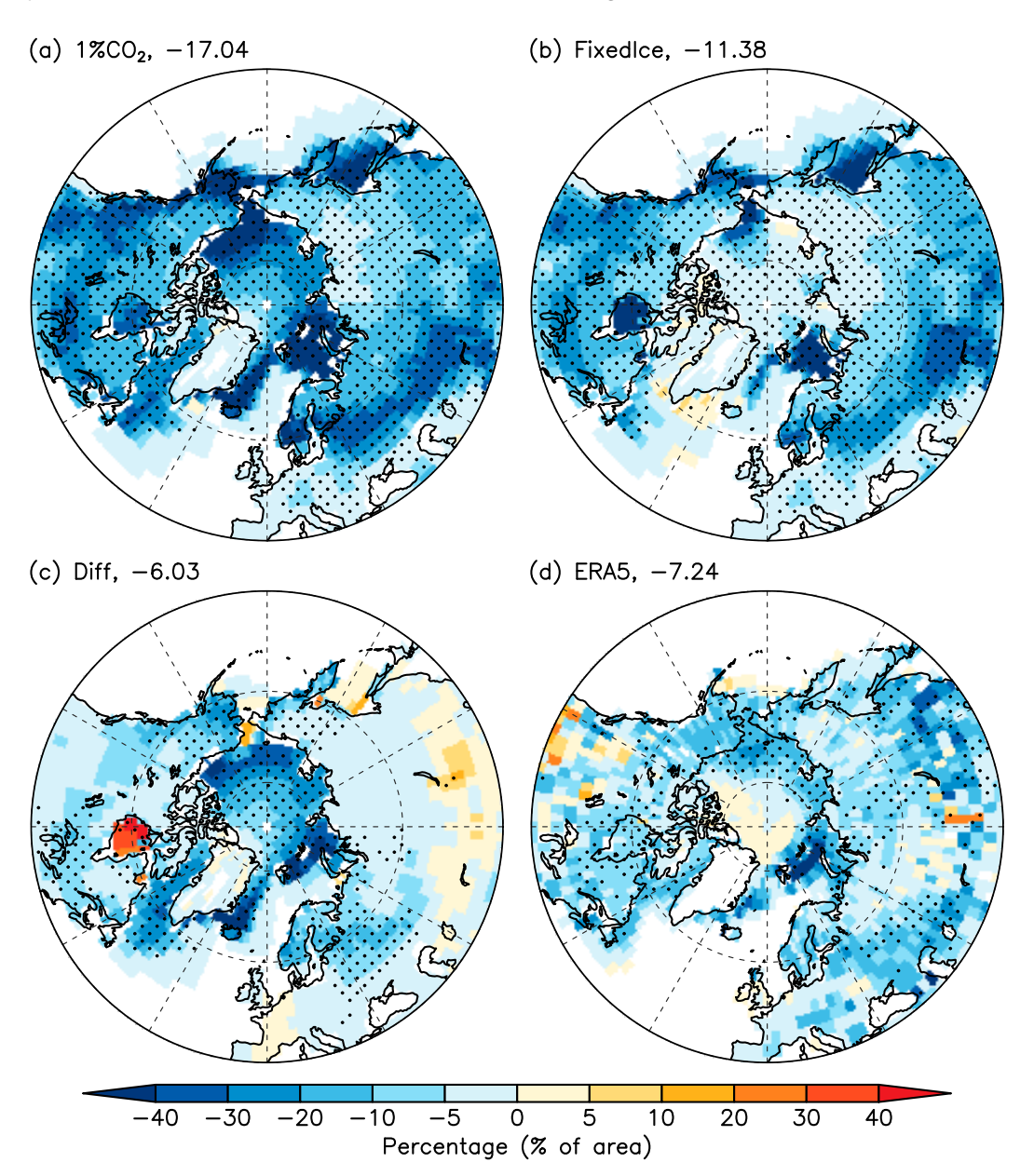


FIG. 11. CESM1-simulated October–March mean changes (relative to the control climatology) in the SIC (over the Arctic Ocean) and snow cover (over land) (% of area) over 40° – 90° N from the (a) 1%CO2 and (b) FixedIce runs and (c) their difference (i.e., 1%CO₂ minus FixedIce) averaged over years 131–150 (around the second CO₂ doubling). (d) As in (c), but for the differences between the 10 years with the lowest and highest Arctic sea ice cover (i.e., low minus high SIC years) based on ERA5 data during 1979–2020. The domain average is given at the top of each panel. The stippling indicates the change or difference is statistically significant at the 5% level based on a Student's t test.

pattern throughout the troposphere within $\sim 20^{\circ}$ –80°N that is collocated with the change pattern in the zonal temperature gradient dT/dx, suggesting that this v change pattern is likely related to the different warming rates over land and ocean in the Northern Hemisphere.

The primary cause of the T variability decrease is the reduced thermal advection -v(dT/dy) and its variance, with the latter resulting mainly from reduced variability of dT/dy with a

small contribution from reduced variability in v. As T variability decreases, the variability of dT/dy also decreases, which in turn decreases the variability of -v(dT/dy), leading to a further reduction in T variability. This provides a positive feedback loop that amplifies the T variability decrease initiated by a reduction in mean dT/dy (from AA) or in the variability of v (caused by the CO_2 forcing). Thus, the AA's influence on midlatitude temperature variability comes mainly from its

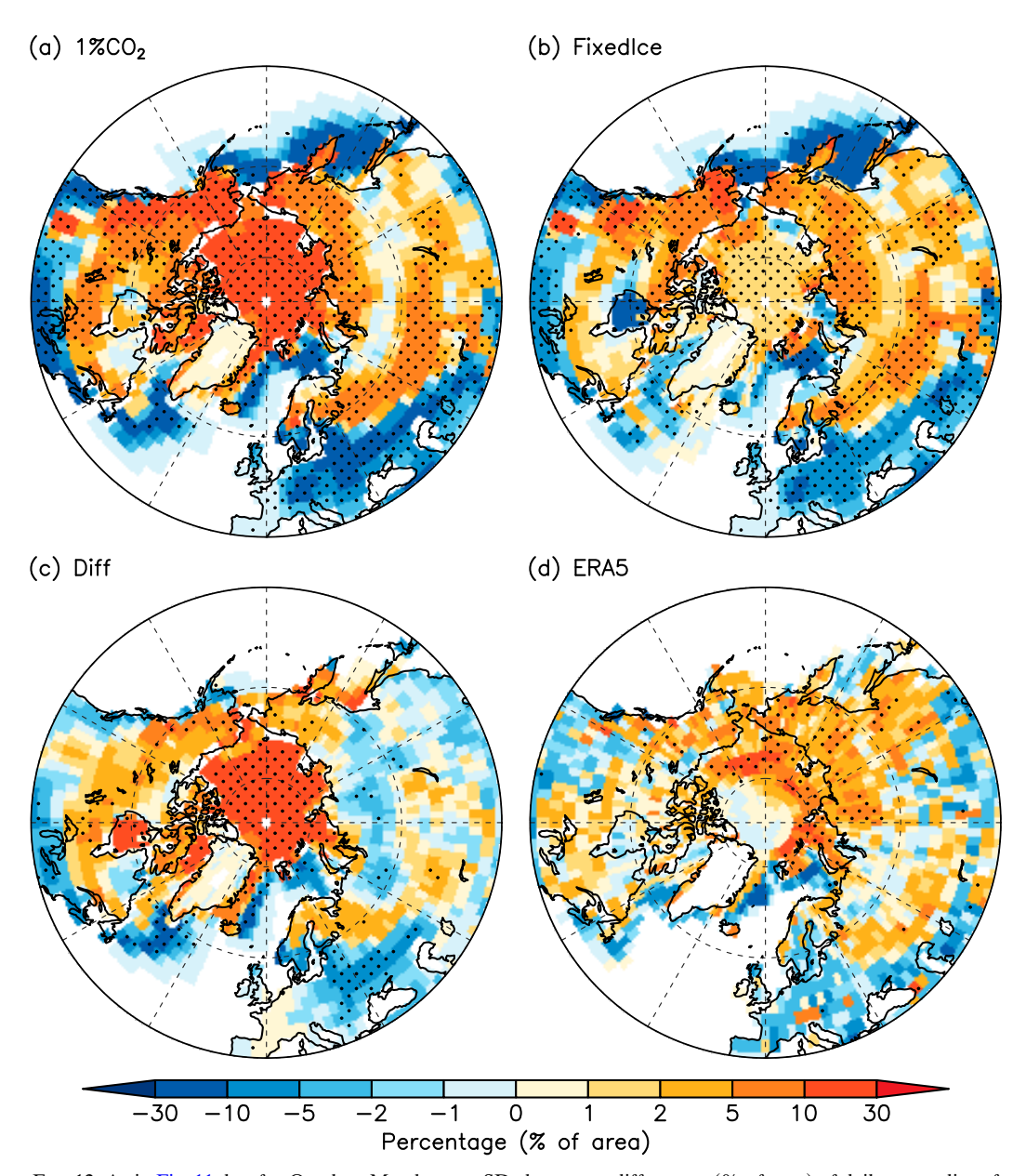


FIG. 12. As in Fig. 11, but for October–March mean SD changes or differences (% of area) of daily anomalies of Arctic SIC and land snow cover.

impact on thermal advection, rather than its dynamic impact on winds. Even though the v wind plays a role in the thermal advection term -v(dT/dy), their changes have different impacts on T variability, with the thermal advection change dominating over the impact from the v change. Thus, focusing only on AA's dynamic impact on winds while ignoring the thermal advection change, as done in some previous studies (e.g., Francis and Vavrus 2012, 2015), may lead to misleading conclusions regarding T variability change under increasing GHGs with large AA and sea ice loss.

Cold-season mean snow and ice cover over northern latitudes decreases under increasing CO₂, while its variance may

increase over many high-latitude regions as the snow and ice cover decreases to below 100% and thus becomes more variable in a warmer climate. The reduced mean snow cover over land and its increased variability both could lead to higher variability in surface T. However, this effect is likely small compared with the effect from the thermal advection change, resulting in a net reduction in T variability over most northern mid-high latitudes.

The composite differences between the years with low and high Arctic sea ice cover in ERA5 during 1979–2020 are generally consistent with our CESM1 model results regarding the impact of sea ice loss and AA, although some of the results

1 April 2021 DAI AND DENG 2607

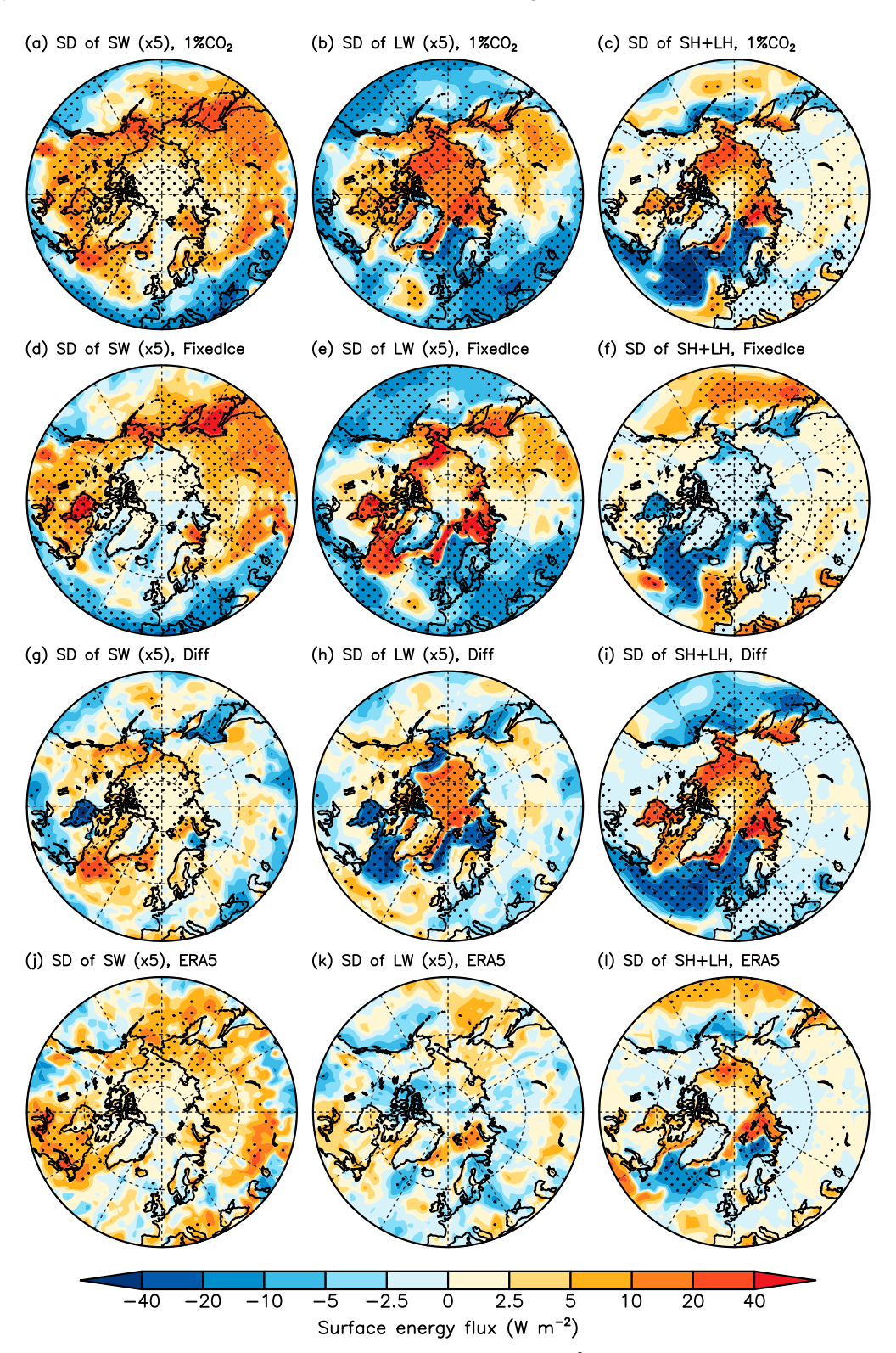


FIG. 13. Spatial distributions of the October–March mean changes (W m⁻²) in the SD of daily anomalies in surface (left) net shortwave (SW) radiation, (center) net longwave (LW) radiation, and (right) turbulent (sensible + latent) heat flux from the (a)–(c) 1%CO₂ and (d)–(f) FixedIce runs and (g)–(i) their difference (i.e., 1%CO₂ minus FixedIce) averaged over years 131–150 (around the second CO₂ doubling). (j)–(l) As in (a)–(c), but for the difference between the 10 years with the lowest and highest Arctic SIC based on ERA5 data during 1979–2020. Note that the changes or differences in surface net SW and LW radiation are multiplied by 5 in order to use the same color bar. The stippling indicates the change or difference is statistically significant at the 5% level based on a Student's *t* test.

2608 JOURNAL OF CLIMATE VOLUME 34

presented here may be model dependent. However, the reduction in T variability over the northern mid-high latitudes is a robust response to increasing GHGs in many other models (Screen 2014; Schneider et al. 2015; Chen et al. 2019), and the impact of the meridional thermal advection -v(dT/dy) is based on the governing equation of T. Thus, we feel confident that the main results reported here are likely to be robust and reliable.

The temperature variability changes may have other implications besides those for temperature extremes. For example, model-projected warming patterns in the twenty-first century are linked to recent temperature variability patterns (Dai 2016), which suggests similar underlying physical processes for the recent temperature variability and twenty-first-century response to GHG forcing. The change in future variability patterns suggest a change in the underlying physical processes (e.g., reduced sea ice-air interactions), which may also change the future (beyond the twenty-first century) mean response to GHG forcing (e.g., weakened AA) as shown by Dai et al. (2019). Furthermore, many other variables, such as atmospheric water vapor and precipitation, closely depend on air temperature; as the temperature variability decreases over the northern mid-high latitudes, the variability in these related variables may also decrease. Further investigations are needed to examine such an effect on other fields.

Acknowledgments. This work was jointly supported by the National Natural Science Foundation of China (Grant 41705054), Natural Science Foundation of Jiangsu Province (Grant BK20170942), Startup Foundation for Introducing Talent of NUIST (Grant 2016r051), Priority Academic Program Development of Jiangsu Higher Education Institutions (PAPD), and China Scholarship Council (Grant 201808320137). A. Dai was supported by the National Science Foundation (Awards AGS-2015780 and OISE-1743738) and the U.S. National Oceanic and Atmospheric Administration (Award NA18OAR4310425).

REFERENCES

- Barnes, E. A., and L. M. Polvani, 2015: CMIP5 projections of Arctic amplification, of the North American/North Atlantic circulation, and of their relationship. J. Climate, 28, 5254–5271, https://doi.org/10.1175/JCLI-D-14-00589.1.
- ——, and J. A. Screen, 2015: The impact of Arctic warming on the midlatitude jet-stream: Can it? Has it? Will it? Wiley Interdiscip. Rev.: Climate Change, 6, 277–286, https://doi.org/10.1002/wcc.337.
- Blackport, R., and J. A. Screen, 2020: Insignificant effect of Arctic amplification on the amplitude of midlatitude atmospheric waves. *Sci. Adv.*, **6**, eaay2880, https://doi.org/10.1126/sciadv.aay2880.
- Chen, J., A. Dai, and Y. Zhang, 2019: Projected changes in daily variability and seasonal cycle of near-surface air temperature over the globe during the twenty-first century. *J. Climate*, 32, 8537–8561, https://doi.org/10.1175/JCLI-D-19-0438.1.
- Cohen, J., and Coauthors, 2014: Recent Arctic amplification and extreme mid-latitude weather. *Nat. Geosci.*, 7, 627–637, https:// doi.org/10.1038/ngeo2234.
- —, and Coauthors, 2020: Divergent consensuses on Arctic amplification influence on midlatitude severe winter weather. *Nat. Climate Change*, **10**, 20–29, https://doi.org/10.1038/s41558-019-0662-y.

- Collins, M., and Coauthors, 2013: Long-term climate change: Projections, commitments and irreversibility. Climate Change 2013: The Physical Science Basis, T. F. Stocker et al., Eds., Cambridge University Press, 1029–1136.
- Collow, T. W., W. Wang, and A. Kumar, 2019: Reduction in northern midlatitude 2-m temperature variability due to Arctic sea ice loss. J. Climate, 32, 5021–5035, https://doi.org/ 10.1175/JCLI-D-18-0692.1.
- Dai, A., 2016: Future warming patterns linked to today's climate variability. Sci. Rep., 6, 19110, https://doi.org/10.1038/srep19110.
- —, and M. Song, 2020: Little influence of Arctic amplification on midlatitude climate. *Nat. Climate Change*, **10**, 231–237, https:// doi.org/10.1038/s41558-020-0694-3.
- —, D. Luo, M. Song, and J. Liu, 2019: Arctic amplification is caused by sea-ice loss under increasing CO₂. *Nat. Commun.*, 10, 121, https://doi.org/10.1038/s41467-018-07954-9.
- Deng, J., A. Dai, and D. Chyi, 2020: Northern Hemisphere winter air temperature patterns and their associated atmospheric and ocean conditions. *J. Climate*, 33, 6165–6186, https://doi.org/ 10.1175/JCLI-D-19-0533.1.
- Deser, C., R. A. Tomas, and L. Sun, 2015: The role of oceanatmosphere coupling in the zonal-mean atmospheric response to Arctic sea ice loss. J. Climate, 28, 2168–2186, https://doi.org/ 10.1175/JCLI-D-14-00325.1.
- Francis, J. A., 2017: Why are Arctic linkages to extreme weather still up in the air? *Bull. Amer. Meteor. Soc.*, **98**, 2551–2557, https://doi.org/10.1175/BAMS-D-17-0006.1.
- —, and S. J. Vavrus, 2012: Evidence linking Arctic amplification to extreme weather in mid-latitudes. *Geophys. Res. Lett.*, 39, L06801, https://doi.org/10.1029/2012GL051000.
- —, and —, 2015: Evidence for a wavier jet stream in response to rapid Arctic warming. *Environ. Res. Lett.*, **10**, 014005, https://doi.org/10.1088/1748-9326/10/1/014005.
- ——, and J. Cohen, 2017: Amplified Arctic warming and midlatitude weather: New perspectives on emerging connections. *Wiley Interdiscip. Rev.: Climate Change*, **8**, e474, https://doi.org/10.1002/wcc.474.
- Garfinkel, C. I., and N. Harnik, 2017: The non-Gaussianity and spatial asymmetry of temperature extremes relative to the storm track: The role of horizontal advection. *J. Climate*, **30**, 445–464, https://doi.org/10.1175/JCLI-D-15-0806.1.
- Hansen, J., M. Sato, and R. Ruedy, 2012: Perception of climate change. Proc. Natl. Acad. Sci. USA, 109, E2415–E2423, https:// doi.org/10.1073/pnas.1205276109.
- Hersbach, H., and Coauthors, 2020: The ERA5 global reanalysis. *Quart. J. Roy. Meteor. Soc.*, **146**, 1999–2049, https://doi.org/10.1002/qj.3803.
- Holland, M. M., and C. M. Bitz, 2003: Polar amplification of climate change in coupled models. *Climate Dyn.*, 21, 221–232, https://doi.org/10.1007/s00382-003-0332-6.
- Holmes, C. R., T. Woollings, E. Hawkins, and H. de Vries, 2016: Robust future changes in temperature variability under greenhouse gas forcing and the relationship with thermal advection. J. Climate, 29, 2221–2236, https://doi.org/10.1175/JCLI-D-14-00735.1.
- Huntingford, C., P. D. Jones, V. N. Livina, T. M. Lenton, and P. M. Cox, 2013: No increase in global temperature variability despite changing regional patterns. *Nature*, 500, 327–330, https://doi.org/10.1038/nature12310.
- Hurrell, J. W., and Coauthors, 2013: The Community Earth System Model: A framework for collaborative research. *Bull. Amer. Meteor. Soc.*, 94, 1339–1360, https://doi.org/10.1175/BAMS-D-12-00121.1.

- Jahn, A., and Coauthors, 2012: Late-twentieth-century simulation of Arctic sea ice and ocean properties in the CCSM4. J. Climate, 25, 1431–1452, https://doi.org/10.1175/JCLI-D-11-00201.1.
- Koenigk, T., and Coauthors, 2019: Impact of Arctic sea ice variations on winter temperature anomalies in northern hemispheric land areas. *Climate Dyn.*, 52, 3111–3137, https://doi.org/10.1007/s00382-018-4305-1.
- Luo, B., D. Luo, A. Dai, I. Simmonds, and L. Wu, 2020:Combined influences on North American winter air temperature variability from North Pacific blocking and the North Atlantic Oscillation: Subseasonal and interannual time scales. *J. Climate*, 33, 7101–7123, https://doi.org/10.1175/JCLI-D-19-0327.1.
- Luo, D., Y. Yao, A. Dai, I. Simmonds, and L. Zhong, 2017: Increased quasi stationarity and persistence of winter Ural blocking and Eurasian extreme cold events in response to Arctic warming. Part II: A theoretical explanation. *J. Climate*, 30, 3569–3587, https://doi.org/10.1175/JCLI-D-16-0262.1.
- ——, X. Chen, A. Dai, and I. Simmonds, 2018: Changes in atmospheric blocking circulations linked with winter Arctic sea-ice loss: A new perspective. *J. Climate*, 31, 7661–7678, https://doi.org/10.1175/JCLI-D-18-0040.1.
- Murray, R. J., and I. Simmonds, 1995: Responses of climate and cyclones to reductions in Arctic winter sea ice. *J. Geophys. Res.*, **100**, 4791–4806, https://doi.org/10.1029/94JC02206.
- Raghavendra, A., A. Dai, S. M. Milrad, and S. R. Cloutier-Bisbee, 2019: Floridian heatwaves and extreme precipitation: Future climate projections. *Climate Dyn.*, 52, 495–508, https://doi.org/ 10.1007/s00382-018-4148-9.
- Rahmstorf, S., and D. Coumou, 2011: Increase of extreme events in a warming world. *Proc. Natl. Acad. Sci. USA*, **108**, 17 905–17 909, https://doi.org/10.1073/pnas.1101766108.
- Schneider, T., T. Bischoff, and H. Płotka, 2015: Physics of changes in synoptic midlatitude temperature variability. *J. Climate*, **28**, 2312–2331, https://doi.org/10.1175/JCLI-D-14-00632.1.
- Screen, J. A., 2014: Arctic amplification decreases temperature variance in northern mid- to high-latitudes. *Nat. Climate Change*, 4, 577–582, https://doi.org/10.1038/nclimate2268.
- —, and I. Simmonds, 2010: The central role of diminishing sea ice in recent Arctic temperature amplification. *Nature*, **464**, 1334– 1337, https://doi.org/10.1038/nature09051.
- —, C. Deser, and L. Sun, 2015: Reduced risk of North American cold extremes due to continued Arctic sea ice loss. *Bull. Amer.*

- Meteor. Soc., **96**, 1489–1503, https://doi.org/10.1175/BAMS-D-14-00185.1.
- —, and Coauthors, 2018: Consistency and discrepancy in the atmospheric response to Arctic sea-ice loss across climate models. *Nat. Geosci.*, 11, 155–163, https://doi.org/10.1038/ s41561-018-0059-y.
- Serreze, M. C., and R. G. Barry, 2011: Processes and impacts of Arctic amplification: A research synthesis. *Global Planet. Change*, 77, 85–96, https://doi.org/10.1016/j.gloplacha.2011.03.004.
- ——, A. P. Barrett, J. C. Stroeve, D. M. Kindig, and M. M. Holland, 2009: The emergence of surface-based Arctic amplification. *Cryosphere*, 3, 11–19, https://doi.org/10.5194/tc-3-11-2009.
- Stouffer, R. J., and R. T. Wetherald, 2007: Changes of variability in response to increasing greenhouse gases. Part I: Temperature. J. Climate, 20, 5455–5467, https://doi.org/10.1175/ 2007JCL11384.1.
- Sun, L., C. Deser, R. A. Tomas, and M. Alexander, 2020: Global coupled climate response to polar sea ice loss: Evaluating the effectiveness of different ice-constraining approaches. *Geophys. Res. Lett.*, 47, e2019GL085788, https://doi.org/10.1029/ 2019GL085788.
- Tamarin-Brodsky, T., K. Hodges, B. J. Hoskins, and T. G. Shepherd, 2019: A dynamical perspective on atmospheric temperature variability and its response to climate change. *J. Climate*, 32, 1707–1724, https://doi.org/10.1175/JCLI-D-18-0462.1.
- —, —, and —, 2020: Changes in Northern Hemisphere temperature variability shaped by regional warming patterns. *Nat. Geosci.*, **13**, 414–421, https://doi.org/10.1038/s41561-020-0576-3.
- Westby, R. M., Y. Y. Lee, and R. X. Black, 2013: Anomalous temperature regimes during the cool season: Long-term trends, low-frequency mode modulation, and representation in CMIP5 simulations. *J. Climate*, **26**, 9061–9076, https://doi.org/10.1175/JCLI-D-13-00003.1.
- Yao, Y., D. Luo, A. Dai, and I. Simmonds, 2017: Increased quasistationarity and persistence of Ural blocking and Eurasian extreme cold events in response to Arctic warming. Part I: Insights from observational analyses. *J. Climate*, 30, 3549– 3568, https://doi.org/10.1175/JCLI-D-16-0261.1.
- Ylhäisi, J. S., and J. Räisänen, 2014: Twenty-first century changes in daily temperature variability in CMIP3 climate models. *Int. J. Climatol.*, **34**, 1414–1428, https://doi.org/10.1002/joc.3773.